



Thermal Model for Welding Simulations

Final Report 278-T-07

For Project

Development of Optimized Welding Solutions for X100 Line Pipe Steel

Prepared for the

Design, Materials, and Construction Technical Committee of
Pipeline Research Council International, Inc.
Project MATH-1 Catalog No. L5XXXX

and

U.S. Department of Transportation
Pipeline and Hazardous Materials Safety Administration
Office of Pipeline Safety
DOT Project BAA DTHP56-07-0001

Prepared by

Yaoshan Chen and Yong-Yi Wang, CRES
Marie Quintana and V.B. Rajan, LECO
Jim Gianetto, CANMET

September 2011

This research was funded in part under the Department of Transportation, Pipeline and Hazardous Materials Safety Administration's Pipeline Safety Research and Development Program. The views and conclusions contained in this document are those of the authors and should not be interpreted as representing the official policies, either expressed or implied, of the Pipeline and Hazardous Materials Safety Administration, or the U.S. Government



Catalog No. L5XXXX

Thermal Model for Welding Simulations

Final Report 278-T-07

Development of Optimized Welding Solutions for X100 Line Pipe Steel

Prepared for the

Design, Materials, and Construction Technical Committee of
Pipeline Research Council International, Inc.

Project MATH-1 Catalog No. L5XXXX

and

U.S. Department of Transportation
Pipeline and Hazardous Materials Safety Administration

Office of Pipeline Safety

DOT Project BAA DTHP56-07-0001

Prepared by

Yaoshan Chen and Yong-Yi Wang, CRES

Marie Quintana and V.B. Rajan, LECO

Jim Gianetto, CANMET

September 2011

Version	Date of Last Revision	Date of Uploading	Comments
2	March 2011	4 April 2011	References to be inserted after review.
Final	September 2011	December 2011	Final Report

This report is furnished to Pipeline Research Council International, Inc. (PRCI) under the terms of PRCI contract [278-PR- 348 - 074513], between PRCI and the MATH-1 contractors:

- Electricore (prime contractor),
- Center for Reliable Energy Systems, CANMET, NIST, and The Lincoln Electric Company (sub-contractors).

The contents of this report are published as received from the MATH-1 contractor and subcontractors. The opinions, findings, and conclusions expressed in the report are those of the authors and not necessarily those of PRCI, its member companies, or their representatives. Publication and dissemination of this report by PRCI should not be considered an endorsement by PRCI of the MATH-1 contractor and subcontractors, or the accuracy or validity of any opinions, findings, or conclusions expressed herein.

In publishing this report, PRCI and the MATH-1 contractors make no warranty or representation, expressed or implied, with respect to the accuracy, completeness, usefulness, or fitness for purpose of the information contained herein, or that the use of any information, method, process, or apparatus disclosed in this report may not infringe on privately owned rights. PRCI and the MATH-1 contractors assume no liability with respect to the use of, or for damages resulting from the use of, any information, method, process, or apparatus disclosed in this report. By accepting the report and utilizing it, you agree to waive any and all claims you may have, resulting from your voluntary use of the report, against PRCI and the MATH-1 contractors.

Pipeline Research Council International Catalog No. L5XXXX

PRCI Reports are Published by Technical Toolboxes, Inc.

3801 Kirby Drive, Suite 520
Houston, Texas 77098
Tel: 713-630-0505
Fax: 713-630-0560
Email: info@ttoolboxes.com

PROJECT PARTICIPANTS

PROJECT TEAM MEMBER	COMPANY AFFILIATION	PROJECT TEAM MEMBER	COMPANY AFFILIATION
Arti Bhatia	Alliance	Jim Costain	GE
Jennifer Klementis	Alliance	Gilmar Batista	Petrobras
Roger Haycraft	Boardwalk	Marcy Saturno de Menezes	Petrobras
David Horsley	BP	Dave Aguiar	PG&E
Mark Hudson	BP	Ken Lorang	PRCI
Ron Shockley	Chevron	Maslat Al-Waranbi	Saudi Aramco
Sam Mishael	Chevron	Paul Lee	SoCalGas
David Wilson	ConocoPhillips	Alan Lambeth	Spectra
Satish Kulkarni	El Paso	Robert Turner	Stupp
Art Meyer	Enbridge	Gilles Richard	TAMSA
Bill Forbes	Enbridge	Noe Mota Solis	TAMSA
Scott Ironside	Enbridge	Philippe Darcis	TAMSA
Sean Keane	Enbridge	Dave Taylor	TransCanada
Laurie Collins	Evraz	Joe Zhou	TransCanada
David de Miranda	Gassco	Jason Skow	TransGas
Adriaan den Herder	Gasunie	Ernesto Cisneros	Tuberia Laguna
Jeff Stetson	GE	Vivek Kashyap	Welpsun
		Chris Brown	Williams

CORE RESEARCH TEAM	
RESEARCHER	COMPANY AFFILIATION
Yaoshan Chen	Center for Reliable Energy Systems
Yong-Yi Wang	Center for Reliable Energy Systems
Ming Liu	Center for Reliable Energy Systems
Dave Fink	Lincoln Electric Company
Marie Quintana	Lincoln Electric Company
Vaidyanath Rajan	Lincoln Electric Company
Joe Daniel	Lincoln Electric Company
Radhika Panday	Lincoln Electric Company
James Gianetto	CANMET Materials Technology Laboratory
John Bowker	CANMET Materials Technology Laboratory
Bill Tyson	CANMET Materials Technology Laboratory
Guowu Shen	CANMET Materials Technology Laboratory
Dong Park	CANMET Materials Technology Laboratory
Timothy Weeks	National Institute of Standards and Technology
Mark Richards	National Institute of Standards and Technology
Dave McColskey	National Institute of Standards and Technology
Enrico Lucon	National Institute of Standards and Technology
John Hammond	Consultant Metallurgist & Welding Engineer

This Page Intentionally Left Blank

FINAL REPORT STRUCTURE

Focus Area 1 - Update of Weld Design, Testing, and Assessment Procedures for High Strength Pipelines		
Report #	Description	Lead Authors
277-T-01	Background of Linepipe Specifications	CRES/CANMET
277-T-02	Background of All-Weld Metal Tensile Test Protocol	CANMET/Lincoln
277-T-03	Development of Procedure for Low-Constraint Toughness Testing Using a Single-Specimen Technique	CANMET/CRES
277-T-04	Summary of Publications: Single-Edge Notched Tension SE(T) Tests	CANMET
277-T-05	Small Scale Tensile, Charpy V-Notch, and Fracture Toughness Tests	CANMET/NIST
277-T-06	Small Scale Low Constraint Fracture Toughness Test Results	CANMET/NIST
277-T-07	Small Scale Low Constraint Fracture Toughness Test Discussion and Analysis	CANMET/NIST
277-T-08	Summary of Mechanical Properties	CANMET
277-T-09	Curved Wide Plate Tests	NIST/CRES
277-T-10	Weld Strength Mismatch Requirements	CRES/CANMET
277-T-11	Curved Wide Plate Test Results and Transferability of Test Specimens	CRES/CANMET
277-S-01	Summary Report 277 Weld Design, Testing, and Assessment Procedures for High Strength Pipelines	CRES

Focus Area 2 - Development of Optimized Welding Solutions for X100 Linepipe Steel		
Report #	Description	Lead Authors
278-T-01	State of The Art Review	Lincoln
278-T-02	Material Selection, Welding and Weld Monitoring	Lincoln/CANMET
278-T-03	Microstructure and Hardness Characterization of Girth Welds	CANMET/Lincoln
278-T-04	Microstructure and Properties of Simulated Weld Metals	CANMET/Lincoln
278-T-05	Microstructure and Properties of Simulated Heat Affected Zones	CANMET/Lincoln
278-T-06	Essential Welding Variables	Lincoln/CANMET
278-T-07	Thermal Model for Welding Simulations	CRES/CANMET
278-T-08	Microstructure Model for Welding Simulations	CRES/CANMET
278-T-09	Application to Other Processes	Lincoln/CANMET
278-S-01	Summary Report 278 Development of Optimized Welding Solutions for X100 Line Pipe Steel	Lincoln

EXECUTIVE SUMMARY

This report was prepared by Center for Reliable Energy Systems (CRES) for the DOT/PRCI co-sponsored project DTPH56-07-T-000005, “Development of Optimized Welding Solutions for X100 Line Pipe Steels.”

As part of the project in Tasks 2, “Identification of Essential Variables”, and Task 3, “Fundamental Understanding of Welding Processes and Essential Variables”, an integrated thermal and microstructure model has been developed to simulate the heat transfer and microstructure changes in gas-metal-arc-welding (GMAW) girth welds. This report summarized the thermal analysis results produced by this integrated numerical model. The numerical model employed a two-dimensional, axis-symmetrical finite element procedure to simulate the transient heat transfer process and the microstructure evolution both in the weld metal and the heat-affected-zone (HAZ). It not only covered the traditional single wire GMAW process, but also has the capabilities to analyze new GMAW processes such as tandem wire and dual torch.

The modeling procedure was implemented using commercial finite element package ABAQUS. The validation of this model was first carried out against the experimental measurements of cooling times and hardness by Mark Hudson. After the implementation of this modeling procedure as a stand-alone simulation software tool, further validations were conducted against thermal cycle measurements made during the two rounds of girth weld fabrications. The comparison between the experimental measurements and the predicted thermal cycles and the cooling times proved that the numerical model was effective, robust, and accurate. With its user-friendly software interface, this software tool was used during the course of the project works to analyze welding procedures, perform virtual experiments to identify welding essential variables, and assist Gleeble simulation test design.

Acknowledgement

This work was jointly funded by PRCI and the U.S. Department of Transportation, Pipeline and Hazardous Materials Safety Administration (PHMSA)’s Pipeline Safety Research and Development. CRES would like to gratefully acknowledge the valuable supports and suggestions received from its project partners: Lincoln Electric, CANMET, BP, and TransCanada. The authors wish to thank Dr. Mark Hudson for granting permission to use his experimental test data and materials in his excellent Ph. D. Thesis.

The views and conclusions contained in this report are those of the authors and should not be interpreted as representing the official policies, either expressed or implied, of the PHMSA, the U.S. Government, or any other funding partners.

TABLE OF CONTENTS

EXECUTIVE SUMMARY	vii
TABLE OF CONTENTS.....	viii
LIST OF FIGURES	ix
LIST OF TABLES	xi
1 Introduction	1
1.1 Heat Transfer in Welding Processes	1
1.2 Gas-Metal-Arc Welding (GMAW) Processes and its High-Productivity Variants	2
1.3 Essential Variables in GMAW for X100 Pipeline Welding	5
2 Objectives and Work Plan.....	6
2.1 Objectives.....	6
2.2 Work Plan.....	7
3 Technical Approach and Implementation of Thermal Model.....	8
3.1 Technical Approach for Thermal Model.....	8
3.2 Numerical Implementation of Thermal Model	14
4 Verification and Applications of Thermal Model	19
4.1 Verification of Thermal Analysis Procedure with Hudson’s Thermal Data	20
4.2 Verification of Thermal Model with First Round Girth Welds	32
4.3 Verification of Thermal Model with Second Round Girth Welds	35
4.4 Virtual Experiments and Identification of Essential Variables	38
4.5 Prediction of Cooling Times for Dual Torch GMAW	48
4.6 Simulation Results for Experimental Plate Welds	49
5 Concluding Remarks	50
5.1 Thermal Modeling of Multi-Pass, Multi-Wire P-GMAW Process	51
5.2 Impact of True Heat Input.....	51
5.3 Characteristics of Thermal Cycles in Multi-wire P-GMAW	51
5.4 The Thermal Analysis Tool.....	52
6 References	53

LIST OF FIGURES

Figure 1. GMAW Process.....	2
Figure 2. A typical pipeline girth weld.	3
Figure 3. A dual-tandem GMAW welding head.....	3
Figure 4. Typical GMAW girth weld bevel in pipeline construction (courtesy of M. Hudson).	4
Figure 5. Work flow of thermal model development, verification, and applications.	8
Figure 6. Narrow groove, multi-pass girth weld and its finite element mesh.....	9
Figure 7. Correlation of weld bead sizes with welding parameters, n[2].	11
Figure 8. Thermal conductivity and specific heat of metal as functions of temperature.....	12
Figure 9. Determination of characteristic times for heat flux model with moving-source solution.	13
Figure 10. Input file for welding simulation of X100 pipeline girth weld.	16
Figure 11. Predicted thermal cycles by stand-alone analysis software with different time increments and their comparison to ABAQUS prediction.	17
Figure 12. Flow diagram of thermal simulation for GMAW girth weld.	18
Figure 13. Microsoft Windows® interface of the thermal analysis software.....	19
Figure 14. A multi-pass P-GMAW girth weld and its corresponding finite element mesh.....	20
Figure 15. Cavity radiation in narrow groove P-GMAW.....	21
Figure 16. Cross-sectional view of single wire P-GMAW showing thermocouple placement.	22
Figure 17. Comparisons of cooling time T85 between measurements and prediction for single-wire P-GMAW with different preheat temperatures.	24
Figure 18. Comparisons of cooling time T84 between measurements and prediction for single wire P-GMAW with different preheat temperatures.	24
Figure 19. Comparisons of cooling time T83 between measurements and prediction for single wire P-GMAW with different preheat temperatures.	25
Figure 20. HAZ regions (colored) produced by single wire P-GMAW process under different pre-heat temperatures.....	26
Figure 21. Sketch of dual torch GMAW process and thermocouple placements.....	26
Figure 22. Finite element mesh for P-GMAW process variation trial. Colored weld regions represent weld metals deposited by different electrode wires.	27
Figure 23. Comparisons of cooling time T85 between measurements and prediction for different GMAW processes.	28
Figure 24. Comparisons of cooling time T84 between measurements and prediction for different GMAW processes.	29
Figure 25. Comparisons of cooling time T83 between measurements and prediction for different GMAW processes.	29
Figure 26. HAZ regions (colored) produced by single wire, tandem wire, and dual torch processes.	30
Figure 27. Two locations in the weld metals deposited by the dual torch in one pass. Green is by the leading torch, blue is by the trailing torch.	30

Figure 28. Thermal cycles experienced by two locations shown in Figure 27 during dual torch welding.	31
Figure 29. Temperature contour after the leading torch and right before the trailing torch for dual torch GMAW process.	31
Figure 30. Section view of HAZ thermocouple in first round girth weld 807K. White region indicates the drilled hole for thermocouple.	32
Figure 31. Location of thermocouple (F5A) for the temperature measurements for weld 807J. ...	33
Figure 32. Comparison of measured and predicted thermal cycles at location shown in Figure 31. Curves with solid lines are by model prediction and dashed lines by thermocouple measurements.	33
Figure 33. HAZ Thermocouple (F2A) location targeting fill pass 2 (right) and partition of girth weld by the thermal model. Red dot indicates the monitoring location for thermal cycles in the model.	34
Figure 34. Comparison between measured thermal cycle for fill pass 1 and predicted thermal cycles with “averaged” heat inputs and true heat inputs.	34
Figure 35. Comparison between measured thermal cycle for fill pass 2 and predicted thermal cycles with “averaged” heat inputs and true heat inputs.	35
Figure 36. Measured thermal cycles from plunged thermocouples for weld 883J.	36
Figure 37. Measured and predicted thermal cycles in HAZ of girth weld made with dual torch P-GMAW.	38
Figure 38. Simulated thermal cycles for case 9 of the virtual experiment.	44
Figure 39. Predicted hardness profile along weld centerline for case 9 of the virtual experiment.	45
Figure 40. Simulated thermal cycles for case 13 of the virtual experiment.	46
Figure 41. Predicted hardness profile along weld centerline for case 13 of the virtual experiment.	46
Figure 42. Macrograph (left) and predicted weld profile (right) by thermal model for experimental plate weld.	50

LIST OF TABLES

Table 1. Measured (M) and Predicted (P) Cooling Times for the preheat trials.	23
Table 2. Measured and predicted cooling times for the process variation trials.....	28
Table 3. Welding conditions for weld 807J.....	32
Table 4. Welding conditions for weld 883J.....	36
Table 5. Comparison of measured and predicted cooling times T_{85} and T_{84} for weld 883J.	37
Table 6. Welding conditions for dual-torch weld 883H.	37
Table 7. Virtual Experiment Matrix.....	40
Table 8. Welding Procedure A.....	41
Table 9. Welding Procedure B.....	41
Table 10. Welding Procedure C.....	41
Table 11. Welding Procedure D.....	42
Table 12. Welding Procedure E.....	42
Table 13. Welding Procedure F.	42
Table 14. Welding Procedure G.....	43
Table 15. Welding Procedure H.....	43
Table 16. Virtual Experiment: Summary of cooling times for single torch GMAW processes.	47
Table 17. Virtual Experiment: Summary of cooling times for dual-torch GMAW processes.	48
Table 18. Welding parameters for dual-torch GMAW.....	49
Table 19. Cooling time results for dual torch simulation.	49
Table 20. Welding parameters for experimental plate weld.	50

1 Introduction

1.1 Heat Transfer in Welding Processes

Over the past two decades, high strength, micro-alloyed, thermo-mechanically processed steels have been developed for modern pipeline constructions because of the advantages of lower weight, lower manufacturing cost, and ease of handling and transportation. Welding of these high strength steels poses a number of challenges due to their sensitivity to the welding parameters such as heat input, preheat temperature, etc. Two primary mechanical properties of the welds are yield strength and toughness. They are directly related to the final microstructures of the welds. Given the chemical composition of the welding consumables and the welding parameters, the microstructure is dependent on the thermal cycles that the weld metals are subjected to during the welding process. In addition, the base metal in the heat-affected zone (HAZ) of the weld also undergoes microstructure changes. These changes in the HAZ, like those in the weld metal, are dependent on the local thermal cycles too. In order to understand the complicated interactions of many factors, an accurate knowledge of the thermal cycles in the weld metal and its HAZ is necessary.

Thermal cycles in welding processes are critical information for process design, control, and monitoring. Unfortunately, due to the high temperature environment, direct contact measurement of the temperature inside the molten weld metal is prohibitive, and new innovative non-contact techniques often include unknown errors that are difficult to determine. Consequently, thermal modeling of welding processes has been an active research area for decades. The early thermal models for welding processes started with Rosenthal's moving source theory^[1] which treated the welding electrode as a moving point source of energy. In an infinite medium, the classic conduction equation gives an analytical solution. Later, this simple solution was expanded to more complicated forms to cover the situations where distributed heat source^[2], finite medium size^[3], temperature-dependent material properties^[4], or phase change^[5] are present. During the 1980's, it was recognized that fluid flow played an important role in determining the final shape of the weld pool. Consequently, sophisticated CFD models were developed to simulate the multi-physics phenomena of fluid flow, heat and mass transfer, electromagnetic field, and surface tension in the weld pool^[6,7].

For different welding processes, the characteristics of heating sources, the mass transfer modes of molten metal and the temperature profiles for heating and cooling cycles can be different. For modern pipeline constructions, welding involves three main groups:

- 1) Mainline welding;
- 2) Tie-in welding for river/road/rail crossings, branch connections, and transition of pipe diameters;
- 3) Repair welding.

Among many arc welding processes, gas metal arc welding (GMAW) and shield metal arc welding (SMAW) processes have become the most popular choices for mainline girth welds and tie-in and repair welds. While the GMAW process is often mechanized for mainline girth welds, the SMAW process is performed manually for tie-in and repair welds. Since these two popular

welding processes share many characteristics in their heat transfer mechanisms, the following section will focus on the GMAW process and its variants for the descriptions of heat and mass transfer process.

1.2 Gas-Metal-Arc Welding (GMAW) Processes and its High-Productivity Variants

1.2.1 GMAW and Pulsed GMAW

A conventional GMAW process is sketched in Figure 1. It uses a continuous electrode for filler metal and an externally supplied gas or gas mixture for shielding. The heat transfer process is characterized by the heating of the weld pool by the impinging arc and the mass transfer of molten metal droplets of the electrode. Depending on the level of arc current, the mass transfer may have different modes of globular, short-circuiting, spray, and pulsed spray. Traditional GMAW uses a constant voltage power source. This constant-voltage character of the power source allows the self-adjustment ability of the arc length through the changes of arc current and the contact tip to workpiece distance (CTWD). This self-adjustment ability combined with a small diameter wire to be pushed through a flexible conduit makes the GMAW process a natural fit for mechanization.

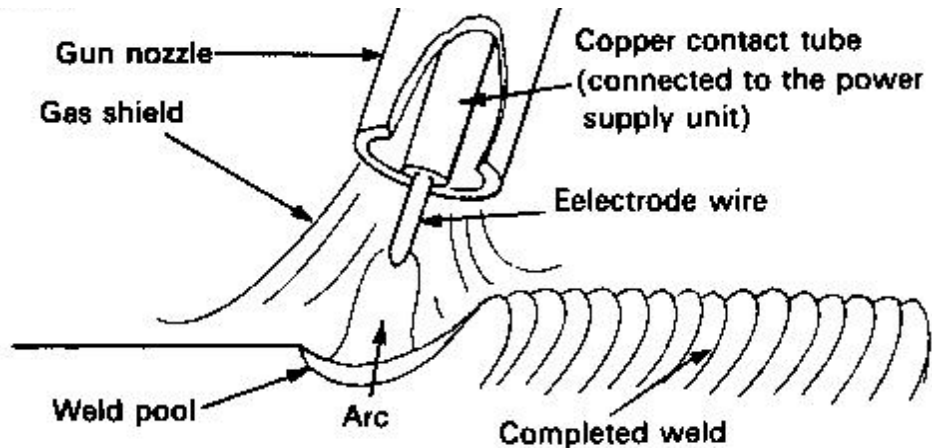


Figure 1. GMAW Process.

Effective GMAW processes often use the short-circuit, globular, or spray modes in their applications as higher arc current in spray mode often leads to poor weld quality due to high heat input (low cooling rates), intense weld pool turbulence, and gas entrainment. Pulsed GMAW (P-GMAW) process was invented in the 1960s to overcome weld problems that were associated with i) fusion defects in short-circuit mode when the arc current is low and ii) low cooling rate in spray mode when the arc current is high^[8]. This was achieved by pulsing the arc current and synchronizing it with the detachment of metal droplets from the welding electrode. The continued development of welding current control has been focused on the flexible and precise control of the pulsed arc current so that extremely smooth, spatter-free welds can be produced with any electrode consumable chemistry and any type of shielding gas.

1.2.2 High Productivity GMAW Processes

As the most widely used welding procedure for large diameter transmission pipelines, a number of variants of GMAW have been developed to increase its productivity. A typical pipeline girth weld, as shown in Figure 2, is made with a number of welding passes, including an internal root pass, an external hot pass, several fill passes, and a final cap pass.

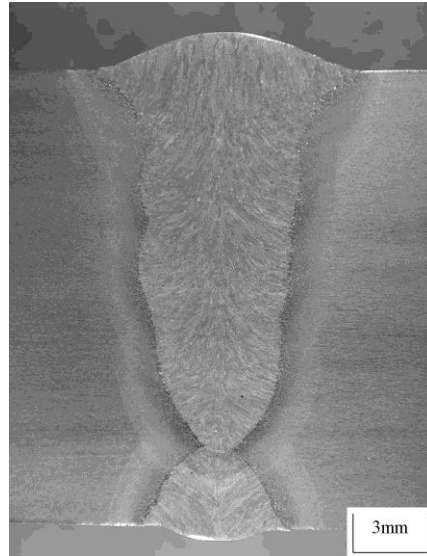


Figure 2. A typical pipeline girth weld.

During field welding in pipeline construction, the root pass welding speed often governs the overall productivity of the pipeline construction, and the welding deposition rates of the fill pass determine the number of welding stations needed to keep pace with the root pass welding. As the pipe wall thickness or the pipe diameter increases, the speed of fill pass welding becomes increasingly important in enhancing productivity.

To increase the welding speed for fill passes, a number of GMAW variants have been successfully developed and applied to both onshore and offshore pipeline constructions ^[9]. These variants include the dual torch GMAW, the tandem GMAW, and the dual-tandem GMAW. The dual-tandem GMAW welding head is shown in Figure 3.

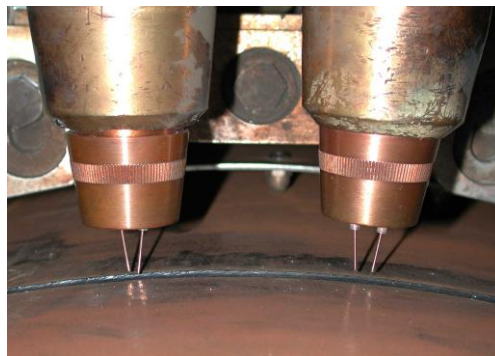


Figure 3. A dual-tandem GMAW welding head.

The traditional GMAW process features a single torch with one electrode wire. The dual torch GMAW process was first designed and used in pipeline construction by Serimax. Similar to the dual-tandem wire system shown in Figure 3, the dual torch system has two torches mounted together on an assembly, but each torch only carries one electrode wire. In a tandem wire GMAW, two consumable wires are passed through the same torch. For both dual torch and dual-tandem wire systems, they require less welding stations since two welding passes can be deposited simultaneously. Among these GMAW variants, the dual torch system has been gaining popularity in pipeline constructions, especially in offshore applications.

Compared to the traditional single wire GMAW, these variant GMAW procedures add more complexity to the heat transfer process. The two electrode wires in the tandem wire GMAW behaves independently in the similar manners in weld metal transfer, but because they are so close to each other (typically 2-4 mm apart depending on wire sizes), a single weld pool is produced. In principle, these two electrode wires can be treated as a single energy source in a heat transfer analysis. For the dual torch system, however, each electrode wire in the two torches produces its own weld pool. As the welding head moves forward, the two weld pools interact with each other.—Depending on the distance between the two torches, the travel speed of the welding process, and the energy power of each electrode wire, the leading weld pool may leave a wide range of temperature fields to the trailing weld pool. Consequently, the weld metal and HAZ regions can experience a variety of temperature cycles.

1.2.3 Narrow Groove Bevel Design of GMAW Girth Welds

Because of the improved fusion characteristics of pulsed GMAW with relative low welding heat input, a narrow groove bevel design is often used for pipeline girth welds. For a typical narrow groove girth weld, its bevel design and welding sequence are depicted in Figure 4.

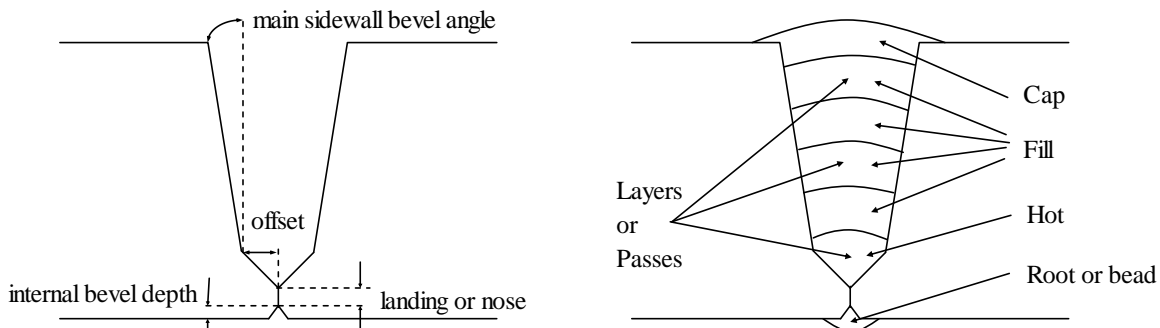


Figure 4. Typical GMAW girth weld bevel in pipeline construction (courtesy of M. Hudson^[10]).

A girth weld made with narrow groove bevel offers many benefits:

- 1) Less consumable consumption;
- 2) Shorter welding times;
- 3) Lower heat inputs for better weld mechanical properties;
- 4) Less welding deformation;
- 5) Lower weld residual stress.

In the development of welding procedure for pipeline construction, great efforts have been taken to overcome issues associated with fusion characteristics such as lack of side-wall penetration and other weld defects. These efforts have included, among others, sophisticated design of pulsed arc current and electrode oscillation.

1.3 Essential Variables in GMAW for X100 Pipeline Welding

1.3.1 Welding Essential Variables

The heat transfer in GMAW is a complex process that includes contributions from many factors. For P-GMAW and its multi-wire variants like dual-torch and tandem wire, more process parameters are added. These new parameters can play important roles like other conventional welding parameters in determining the thermal cycles during welding and the final mechanical properties of the girth welds.

Essential variables in a welding process for certain applications are defined as those welding parameters that have a significant effect on the mechanical properties of the joint. In some industrial standards such as API1104^[11] for pipeline welding, these essential variables are identified and it is required that the welding procedure be re-qualified if any of the essential variables is changed outside of a specified parameter range.

For the present research work, in addition to the conventional welding parameters, three new process-related factors need to be considered for the identification and assessment of essential variables:

- 1) New X100 welding consumable;
- 2) Heat input characterization of the power source; and
- 3) Multi-wire GMAW variants.

1.3.2 X100 Consumable

One of the essential variables in any welding process is the chemical composition of the electrode consumable. In the case of X100 welding, previous research works have shown that the mechanical properties of an X100 girth weld are more sensitive to the welding procedure than those of girth welds made for lower grade linepipes and significant variations in mechanical properties can occur within a weld or from weld to weld. In order to establish a viable range of welding conditions to meet the stringent mechanical properties required for high strain pipeline applications, it is essential to understand the response of the X100 weld consumables to various heating and cooling cycles.

1.3.3 True Heat Input

The second factor needs to be considered is the precise evaluation of heat input for the P-GMAW processes. For a P-GMAW process, as revealed and described in detail in a different topical report of this project, Report 278-T-02^[12], the averaged heat input recorded through the conventional calculation method often misrepresents the true heat input. Since the heat input for

any welding process is a leading essential variable, the influence of the true heat input on the thermal cycles and the weld properties in comparison to the nominal (averaged) heat input needs to be investigated.

1.3.4 Multi-wire P-GMAW Processes

As illustrated before, the multi-wire GMAW processes, in particular, the dual-torch GMAW, have offered the promise of enhanced productivity and indeed become the popular choice for pipeline welding. In the case of dual torch or dual tandem wire where two successive weldpools are present, the compounded thermal cycles and their implications to the final mechanical properties of the welds are not well understood. As a matter of fact, there are not many successful research works on the evaluation of thermal cycles in multi-wire GMAW^[13].

Among the three new factors listed above, the first one is already an essential variable, and its responses and interactions with other welding parameters were to be investigated in the project. The second factor is embodied in the conventional essential variable, heat input, but emerges itself from a new welding condition, the pulsed arc current. It has the potential to become an independent essential variable. The multi-wire GMAW variants, in addition to having multiple sets of welding parameters for each electrode wire, inter-torch parameters, such as the distance between torches, can certainly become essential variables.

To summarize, in order to meet the stringent requirement of mechanical properties of X100 pipeline girth welds, the dependence of welding thermal cycles and microstructures of weld metal and HAZ on welding parameters need to be investigated. Essential parts of this understanding should include the effects of new weld consumables for X100 linepipes, the heat input character of P-GMAW, and the multi-wire P-GMAW variants.

As a part of this effort, an integrated thermal-microstructure model was developed. In the remaining parts of this report, the objectives for the development of the thermal model, the technical approach for its development, the verification and prediction results of the thermal model are presented.

2 Objectives and Work Plan

2.1 Objectives

As a part of the project, an analysis tool was needed to predict the thermal cycles and microstructures of the weld metal, the heat-affect zone (HAZ), and the base metal. Specifically, an integrated thermal-microstructure finite element model was developed. Toward the overall objectives of the project, this integrated numerical model served multiple purposes during the overall execution of the project:

- 1) Help understand the effects of welding parameters, including those related to true heat input, multi-wire P-GMAW;
- 2) Help identify the essential variables of X100 welding process through virtual experiments;
- 3) Help welding procedure design, perform results predictions, and evaluate welding results.

It was realized from the start of the project that the model would be developed mainly for the evaluation of X100 pipeline girth welds, although the model can be modified readily to cover other pipeline welding processes such as SMAW for tie-in or even seam welding during pipe manufacturing. The model also covers both the traditional single-wire P-GMAW and multi-wire P-GMAW variants.

It was also realized that the thermal model, integrated with the microstructure model, should serve as an efficient tool to perform a large number of simulations and virtual experiments. Each analysis or modeling case requires a significant amount of effort to set up the input parameters, meshing, and procedure tuning if using a third-party finite element package. Consequently, in its final form, it was developed as a stand-alone numerical simulation software tool, rather than relying on third-party finite element software.

2.2 Work Plan

In developing the thermal model, a number of steps were taken in order to establish the analysis procedure, calibrate and verify the thermal model, and perform virtual experiments and welding result predictions. Along each of the steps, the development and use of this thermal model were assisted with prior-existing thermal cycle measurement data, thermal cycle data obtained during trial plate welding, two rounds of pipe girth welding, plate welding for the welding procedure design of the final round of girth welds. These steps include:

- 1) Development and verification of the thermal analysis procedure with ABAQUS, a commercial finite element package;
- 2) Implementation of the thermal analysis procedure into a stand-alone analysis software tool;
- 3) Calibration and verification of the thermal model with the first round of girth welds;
- 4) Calibration and verification of the thermal model with the second round of girth welds;
- 5) Virtual experiments and identification of essential variables;
- 6) Simulation and prediction of plate welding results.

In addition to the steps taken above, the thermal model was used, after its successful implementation and verification, to assist the welding procedure design and the Gleeble simulation design for weld metal microstructure characterization.

It should be noted that although the microstructure model is reported in a separate topical report, Report 278-T-08^[14], its development, verification, prediction, and use were closely integrated with those of the thermal model.

The work flow for the thermal model development, its verification and applications in the research activities is illustrated in Figure 5. The origins of the arrows indicate where the inputs are from, and the ends of the arrows indicate what the works lead to.

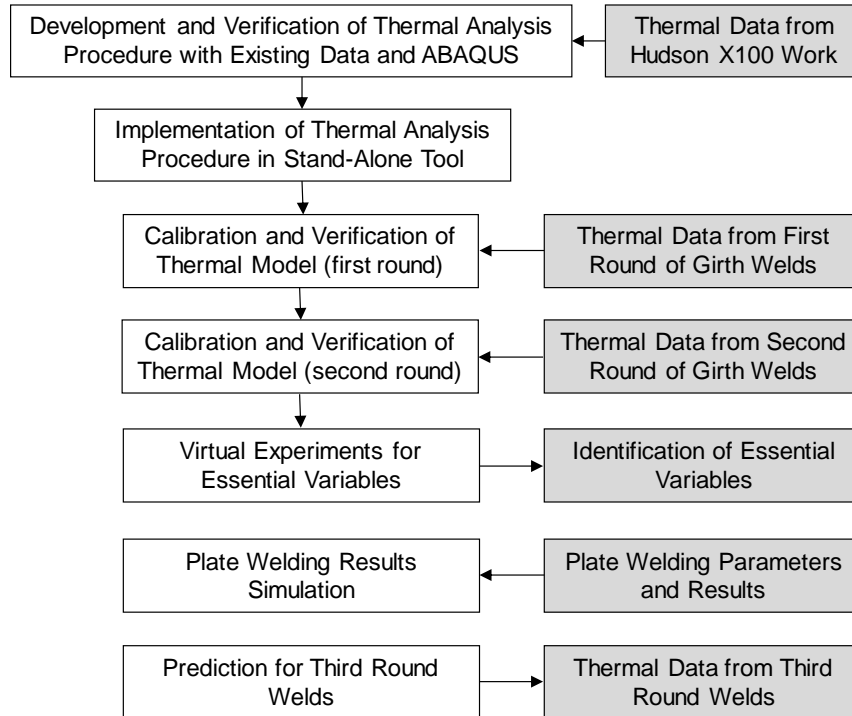


Figure 5. Work flow of thermal model development, verification, and applications.

3 Technical Approach and Implementation of Thermal Model

In this section, the technical approach for the development of the thermal analysis procedure is first presented. As stated in the previous section, the development and verification of this procedure was carried out using the commercial finite element package ABAQUS. Since this part of the model development effort was started early, it used the thermal measurement data from Hudson^[10] for its verification.

After the development and verification against existing measurement data, the analysis procedure was implemented with generic finite element procedure to produce a stand-alone software tool. The details of this implementation, its structure, components, and usage are described in the second half of this section.

3.1 Technical Approach for Thermal Model

3.1.1 An Overview

Thermal simulation of welding process has continuously been an active research area because of the ubiquitous applications of welding processes. From the Rosenthal's pioneering moving-source solution to the latest three-dimensional computational fluid dynamics (CFD) models that accounted for the heat conduction in the solid metal, the fluid flow in the weldpool, and the arc-pool interaction, etc., numerical models with different levels of sophistications have been proposed and developed for different applications.

For multi-pass and multi-wire P-GMAW girth welds in pipeline construction, the application of these sophisticated 3D models is computationally impossible because in addition to the expensive computational algorithms, a large three-dimensional finite element mesh is needed to resolve the thermal fields in each pass. It becomes even more difficult when the dual torch GMAW is modeled because compared to a single torch situation, the two torches requires a much larger computational domain (depending on the torch distance) and the same level of mesh refinement as that of the single torch model. Consequently, simplified, two-dimensional, conduction-based thermal models become the viable candidate for thermal analyses if a large number of welding simulations need to be performed efficiently. Some of the conduction-based finite element thermal models with distributed heat sources, Goldak's double ellipsoid heat source model^[15], for instance, have proven to be quite effective for residual stress and distortion calculations and other welding-related analyses. This methodology has been applied to many two-dimensional models for P-GMAW welding processes for its efficiency. Modifications to this two-dimensional implementation have been proposed to further improve its robustness and consistency^[16]. As a key feature of the modeling procedure, the heat flux provided by the electrode/arc is often applied through a trial-and-error approach by varying its intensity so that the weld metal region as a whole goes through a molten state. For a pipeline girth weld made with multiple passes and sometimes with multiple electrodes, however, the implementation of this numerical approach can be very cumbersome and inconsistent because of the differences in the areas and geometries of the weld passes. Therefore, in order to perform thermal analyses for the girth welds accurately and efficiently, a self-consistent and robust heat-flux model for welding conditions of typical practical range was needed.

In the sections below, the thermal analysis procedure for a multi-pass multi-wire GMAW girth weld is described.

3.1.2 Thermal Model of Multi-pass Multi-Wire GMAW Girth Weld

A mechanized, narrow groove, multi-pass girth weld, as shown in Figure 6 , is usually made with an internal root pass, an external hot pass, and several fill passes. The thermal model assumes that the heat transfer process is axis-symmetrical and symmetrical about the weld centerline. The mesh shown at the right represents the weld region which is partitioned into different passes according to the actual welding sequence. In this work, the root pass is not considered in the model. Each pass of the mesh is associated with a heat flux whose properties are directly derived from the welding parameters of that particular pass.

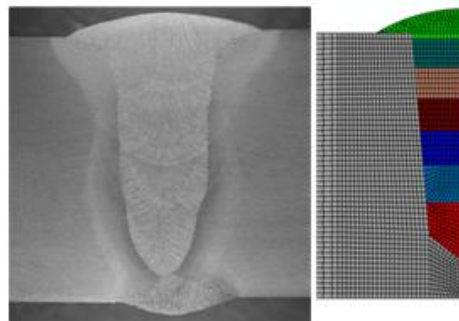


Figure 6. Narrow groove, multi-pass girth weld and its finite element mesh.

For a typical multi-pass, multi-wire P-GMAW girth weld, the axis-symmetrical, transient thermal model consists of a few key components as follows:

- 1) The finite element mesh;
- 2) Material properties needed for temperature calculation;
- 3) The proper presentations of the welding passes as heat fluxes passing through the modeling domain;
- 4) Boundary conditions at the model surfaces.

Finite Element Mesh

The finite element mesh, shown as in Figure 6, was generated based on the following information:

- 1) The pipe dimensions, i.e., diameter and wall thickness;
- 2) The girth weld bevel design with key dimensions including the bevel angle, bevel offset, landing, bevel offset angle, internal bevel depth, and internal bevel angle, as shown in Figure 4. Two additional dimensions are girth weld cap height and cap width. These two dimensions can be assigned from actual measurements of the cap shape of the girth weld.
- 3) The weld parameters for each pass;

Before the mesh was generated, the whole girth weld must be partitioned into regions that represent the welding passes. The area (volume) of each region must be accurately measured according to the welding parameters for the corresponding pass. To calculate the area of a GMAW welding pass, the weld area measurement data in Reference 2 was used to correlate the weld bead sizes and the welding parameters. The plots of weld bead area vs. welding parameter n are shown in Figure 7. Given the information listed above, the area of every welding pass was determined first from the correlation. This area was then adjusted according to global mass conservation calculated from the diameter of the consumable wire and the wire feed speed (WFS). The partitioned weld regions for all the weld passes are meshed, and all elements in each weld pass are properly grouped. Finally, the meshes for other non-weld regions are generated to complete the meshing step.

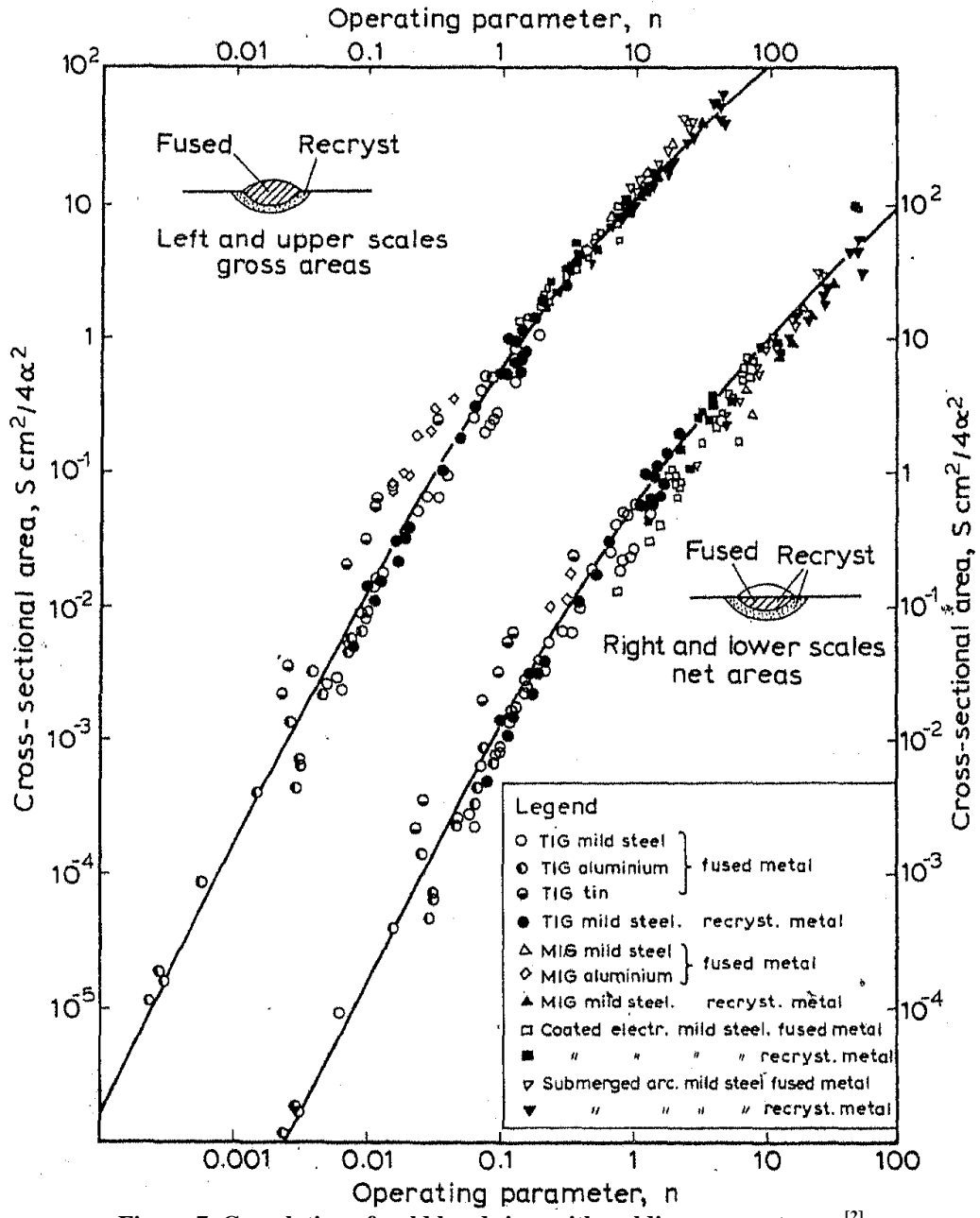


Figure 7. Correlation of weld bead sizes with welding parameters, $n^{[2]}$.

As the welding passes are deposited one after another, the corresponding group of elements must be activated in the right order. In the same time, the “active” external surface of the weld metal and the bevel surfaces are identified and activated accordingly for the applications of boundary conditions.

Thermal Material Properties

The thermal material properties for both weld metal and the base metal were treated as that of low-carbon steel^[17]. The density of the metal is 7800 kg/m³; the solidus temperatures and liquidus temperatures of weld metal and base metal are calculated by the microstructure model from their chemical compositions, respectively; the latent heat for solid-liquid phase change is

247 kJ/kg. The specific heat and the thermal conductivity of the metal are temperature-dependent, and the dependencies are plotted in Figure 8.

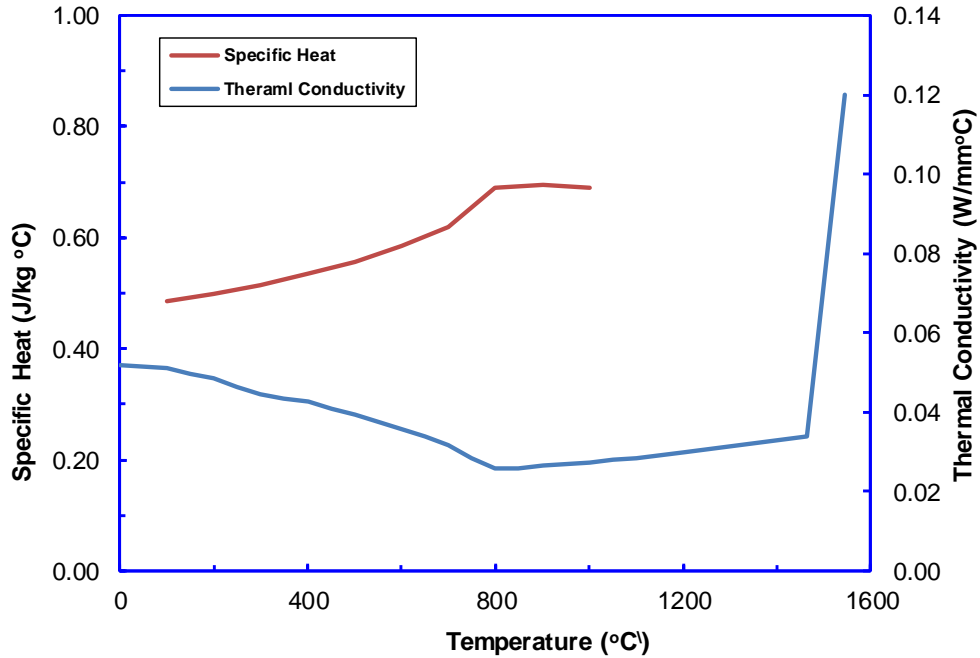


Figure 8. Thermal conductivity and specific heat of metal as functions of temperature.

Heat Flux Model and True Heat Input

To simulate the heat transfer process where a welding pass is in progress, a transient heat flux is applied to the element group that represents the weld pass. As the heat flux sweeps through, it causes a typical heating-cooling temperature cycle in the weld metal and its neighboring area.

To simulate single wire P-GMAW process, the preheat and inter-pass temperatures are maintained at the start of the welding or between two successive weld passes. When dual torch P-GMAW is used, the heat flux by the leading electrode is applied first. After a certain amount of time delay, the heat flux by the trailing electrode is applied. The time delay between the two heat fluxes is determined by the travel speed of the torch assembly and the distance between the two torches.

This heat flux carried by the wire droplets and the welding arc is treated in the finite element model as a body heat source. A spatially uniform distribution of the heat source is assumed across the weld pass section. In the transient 2D thermal model, this uniformly distributed heat source sweeps through the model plane as a function of time in the following form:

$$q(t, t_o, \tau_f, \tau_b) = \begin{cases} Ce^{-(t-t_o)^2/\tau_f^2}, & t \leq t_o \\ Ce^{-(t-t_o)^2/\tau_b^2}, & t > t_o \end{cases} \quad (1)$$

where q is the thermal energy density, C is a constant; t_o is the moment when the peak of the heat flux sweeps through the model plane; τ_f is a characteristic time scale when the electrode is approaching the model plane; τ_b , on the other hand, is the characteristic time scale when the

electrode is leaving the model plane. These two characteristic times are determined by the travel speed of the electrode and the longitudinal lengths of the weld pool before and after the electrode. The two lengths, l_f and l_b as shown in Figure 9, are calculated from the moving-source solution^[1] using the welding parameters for the pass. Constant C is determined through global energy conservation for the electrode:

$$W = \int dt \iint_{weld} q dx dy \quad (2)$$

where the integral is over the weld pass area and the time span it lasts, and W is the total thermal energy for the pass.

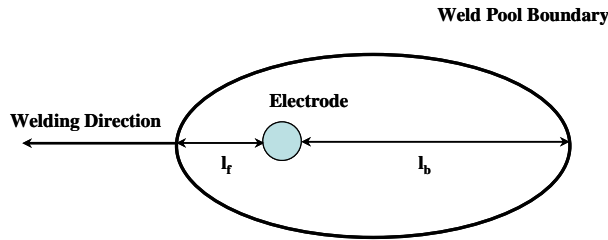


Figure 9. Determination of characteristic times for heat flux model with moving-source solution.

From Equations (1) and (2), it is obvious that detailed weld geometry information for every pass and their corresponding welding parameters are needed if the heat flux calculation is followed rigorously.

For a multi-wire GMAW such as dual torch process, the principle of superimposition was applied in the evaluation of the heat flux, i.e., each electrode or torch is treated as an independent moving heat source formulated according to Eqs. (1) and (2), and is imposed onto its corresponding weld pass region in the same sequence as in the actual welding process. The time delay between these independent heat sources is a function of the distance between them and the welding speed. In mathematical terms, the composite heat fluxes of dual torch can be described as the following:

$$q = q_1 + q_2, \text{ for total heat flux,}$$

$$q_1 = q_1(t, t_{o1}, \tau_{f1}, \tau_{b1}), \text{ for leading torch, and}$$

$$q_2 = q_2(t, t_{o2}, \tau_{f2}, \tau_{b2}), \text{ for trailing torch.}$$

where $t_{o2} - t_{o1} = \Delta t$ is the time delay between the two torches.

In the heat flux formulation described above, the power calculation for each welding pass was based on the averaged heat input of the pass, and a nominal arc efficiency of 90% was assigned in the model. To account for the true heat input, the power of the welding pass was modified according to the specified true heat input as a user input. For example, real time measurement of true heat input from the present project work indicated that the true heat input was 15-20% higher than the averaged heat input. Consequently, an increase of the power for the welding pass was made to enforce the true heat input in the model.

Boundary Conditions

For all boundaries in the finite element model, the conventional free convection and surface radiation conditions were assumed. This heat loss can be written as:

$$q_s = h(T_s - T_o) + \varepsilon\sigma(T_s^4 - T_o^4) \quad (3)$$

where h is the free convection heat transfer coefficient, T_s is the surface temperature in Kelvin, T_o is the environment temperature in Kelvin, ε is the surface emissivity, and σ is the Stefan-Boltzmann constant. The values of these constants are user inputs, and for typical field and pipe conditions, $T_o=300\text{K}$, $h=1\times 10^{-5}\sim 1\times 10^{-4}\text{ J/mm}^2\text{ }^\circ\text{C}$, and $\varepsilon=0.1\sim 0.3$. It is important to note that weld metal is added to the bevel region pass by pass according to the welding sequence, and the change of boundary surfaces due to new weld deposition follows the same order.

3.2 Numerical Implementation of Thermal Model

The thermal analysis procedure described in the previous section was developed first using a commercial finite element package ABAQUS. After its successful development and verification against existing measurement data, the thermal model (together with the microstructure model) was implemented with generic finite element procedure and a stand-alone software tool was produced.

The primary purpose of implementing the thermal model in a finite element procedure is to automate the entire analysis procedure. Compared to the ABAQUS thermal model, the stand-alone analysis software tool offered the following benefits:

- 1) The stand-alone software tool can perform a complicated thermal (and microstructure) analysis process more efficiently than the ABAQUS model. As demonstrated in Section 3.1, the thermal analysis procedure takes a large amount of input information to build the finite element model. Among these inputs, the partitioning of the girth weld as described in Section 3.1 required manual calculations before the finite element mesh could be generated in the ABAQUS model. This partitioning calculation and the ensuing meshing, element grouping and activations, and boundary surface identifications during the transient heat transfer simulation are very time-consuming. Furthermore, any change in pipe dimensions, girth weld bevel dimensions, or welding parameters for one welding pass would require total re-calculation of weld partitioning and re-meshing. Therefore, when a large number of simulations are to be performed, the cost to set up these thermal models would be very high. On the other hand, the automation of the thermal analysis procedure with a finite element method only requires the compilation of a comprehensive input file at the beginning of the simulation.
- 2) For a large number of simulations with different welding conditions, because the automated analysis tool integrated the weld partitioning, mesh generation, and finite element simulation together, it produced more consistent and accurate results than the error-prone ABAQUS modeling procedure.
- 3) During the implementation of the thermal analysis procedure with ABAQUS, it was found that for dual torch GMAW, ABAQUS had trouble handling the activations of the two groups of elements for the leading and trailing wires and the time delays between the

two torches. This was probably due to the limitations of access to ABAQUS user subroutines. The automated analysis tool was very robust in dealing with element activations and successive torch applications because the codes were designed and implemented for these special scenarios.

The entire thermal model was implemented with a generic finite element procedure. The program was written in C++ with an object-oriented structure for the ease of implementation.

3.2.1 Components of the Implementation

The finite element implementation of the thermal model consisted of the following major components:

- 1) The input module;
- 2) The weld partitioning module;
- 3) Heat flux formulation module;
- 4) Transient finite element solver for temperature simulation;
- 5) Output of results.

The Input Module

This component reads a complete set of data for the entire girth weld simulation. The input data includes the following information:

- 1) The case name for this simulation. It is the tag of this simulation. All the output result files are identified with this tag;
- 2) Pipe dimensions, including pipe outer diameter and wall thickness;
- 3) Bevel dimensions, including offset, offset angle, landing, bevel angle;
- 4) Welding parameters
 - a. Number of welding passes;
 - b. For first pass: welding current, voltage, travel speed, arc efficiency
 - c. Wire diameter, wire feed speed, oscillation frequency, oscillation width, CTWD, and dwell time;
 - d. Preheat or inter-pass temperature, simulation time for this pass, torch delay time (if this is a trailing torch otherwise set to -1);
 - e. Repeat items b, c, d for all the passes;
 - f. Cap pass dimension, including its width and height;
- 5) Boundary conditions, including environment temperature, free surface heat transfer coefficient, and surface emissivity;
- 6) Chemical composition for base metal (pipe);
- 7) Chemical compositions for weld metals (multiple weld metals are allowed).

In addition to the input information listed above, the analysis software also reads in simulation control parameters such as increment-step limit, output requests, etc.

```

girthweldinput.txt - Notepad
File Edit Format View Help
CANMET-GL-PT1-v2
1
914.4 19.0
1
2.54 5.0 1.5 52.0
1.04 37.5
1
5
25 188 1346.2 0.9
1.0 10.62 3.5 1.5 13.5 0.0
27 50.0 -1
24 185 508 0.9
1.0 10.64 3.5 1.5 13.5 0.0
27 50.0 -1
24 206 508 0.9
1.0 10.63 3.5 1.5 13.5 0.0
27 50.0 -1
23 194 508 0.9
1.0 10.63 3.5 1.5 13.5 0.0
27 50.0 -1
23 249 228.6 0.9
1.0 10.62 3.5 1.5 13.5 0.0
27 80.0 -1
300 0.00001 0.1
1
0.5 12.66
1
0.068 1.86 0.006 0.005 0.11 0.03 0.53 0.27 0.31 0.042 0.002 0.029 0.009 0.0001 0.000 0.004
1
0.093 1.64 0.013 0.012 0.58 0.22 1.45 0.46 0.103 0.0005 0.004 0.005 0.06 0.0001 0.005 0.000
2
0.025 1.98 0.006 0.005 0.20 0.42 0.48 0.43 0.46 0.006 0.00 0.05 0.015 0.0005 0.0038 0.0050
### the following line explains the elements input (wc%)
C Mn P S Si Cr Ni Mo Cu Al V Nb Ti B O N
## comments and notes for the file, starting from line 1
Top line: the name of this, must be one string with no space between letters
#this block is for weld geometry, depends on the first entry, the type; line 1 and 2
line 1: #type of wele geometry-1, girth weld; 2, plate butt weld; 3, fillet weld (1)
line 2: pipe_diameter, wall_thickness (2)
#second block, bevel information, line 3-5
line 3: type-CRC/RMS...according to Hudson (1)
line 4: bevel_offset, bevel_angle, landing_depth, offset_angle (4)
line 5: internal bevel depth, internal bevel angle (2)
#welding parameters, number of lines depends on the numer of pass and number of materials, starting from

```

Figure 10. Input file for welding simulation of X100 pipeline girth weld.

Girth Weld Partitioning Module

After all the information for welding simulation is read, the partition of the girth weld into sub-regions according to welding parameters associated with each pass is performed. The partition procedure was outlined in Section 3.1.2. This part is crucial for mesh generation in the next step as it lays out the key geometry dimensions for each pass. The correct partitions of welding passes, combined with the heat inputs associated with each pass, is critical to yield thermal cycles that have the right peak temperature. For an active welding pass, for instance, it is essential that all the weld metal go through a peak temperature higher than the melting point of the metal. If the partitioned pass area is too high, the calculated peak temperature will be too low and erroneous “un-molten” weld metal would exist.

Meshing Module

The finite element mesh was generated with unstructured quadrilateral elements. The elements were grouped according to the partitions given in the previous step. They were also tagged according to their material identifications.

As a part of the meshing process, the external surfaces of the model were also identified and properly grouped according to welding sequence. It should be noted that as the welding passes were added to narrow groove, the external surfaces keep changing. This transient behavior of external surfaces must be captured in the model for the applications of boundary conditions as in Section 3.1.

Heat Flux Formulation Module

After the mesh generation, the next step is the characterization of the heat fluxes associated with every welding pass. As in the heat flux formulation presented in Section 3.1, the power of each pass, the characteristic lengths l_f and l_b , and characteristic time scales τ_f and τ_b are evaluated from the welding parameters of the pass.

The correct evaluations of these parameters for the heat flux are critical for the thermal model to capture the right peak temperature of a local thermal cycle. The conventional approach for the evaluation of the heat flux for welding process simulation has been through trial-and-error by adjusting the power intensity of the heat flux until the intended peak temperature is reached. Compared to the traditional approach, the incorporation of moving-source solution in the present heat flux formulation through τ_f and τ_b proved to be instrumental in its success. After extensive calibrations and verifications against measured thermal cycles, this formulation can predict local thermal cycles with the right peak temperatures. It demonstrated its robustness and consistency in its applications to GMAW processes with a reasonably large range of welding conditions.

Transient Finite Element Solver for Temperature Simulation

The finite element solver used the standard numerical procedures for stiff-matrix calculation and global matrix assembly. The Crank-Nicolson scheme was used for the implicit time integral, and the global matrix was solved through an iterative solver along with the Reverse-Cuthill-McKee band reduction algorithm^[18]. The latent heat associated with solid-liquid phase change was included in the finite element calculation through the enthalpy method^[19].

Before its use for welding simulation, the finite element code went through rigorous numerical convergence tests and stability tests. Its computation results were also compared to those by ABAQUS under the approximately same welding conditions. A sample of such a comparison of predicted thermal cycles is shown in Figure 11. It is clear from the plots that with three different time increments, the thermal analysis software gives consistent (almost totally overlapping) predictions of the thermal cycles. The agreement between the analysis software and ABAQUS are reasonably good.

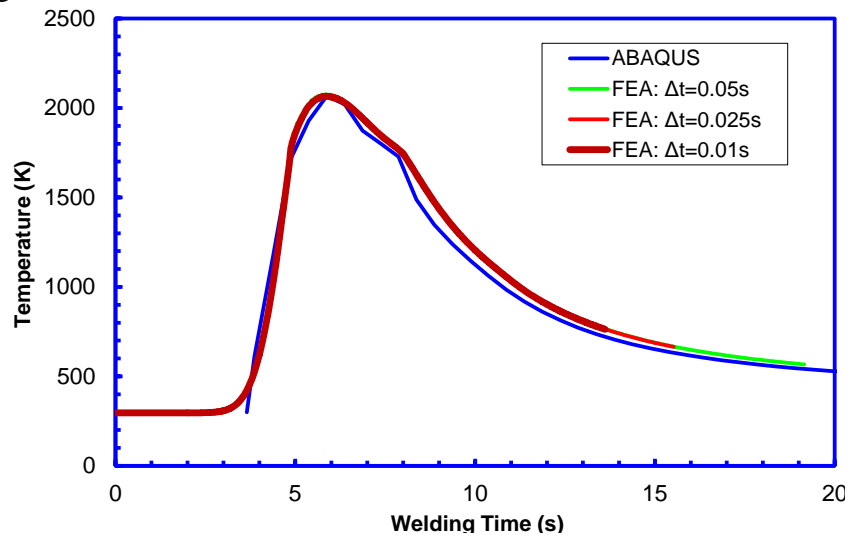


Figure 11. Predicted thermal cycles by stand-alone analysis software with different time increments and their comparison to ABAQUS prediction.

Output of Results

As part of the program outputs, snapshots of peak temperature distributions over the entire model domain are recorded after each pass is completed. In addition, temperature histories at selected locations in weld and HAZ regions are extracted for post-processing. User can also request temperature history outputs at location of their interest. Figure 12 shows the flow diagram of the thermal analysis software (microstructure parts are also included in this diagram) for a multi-pass GMAW girth weld.

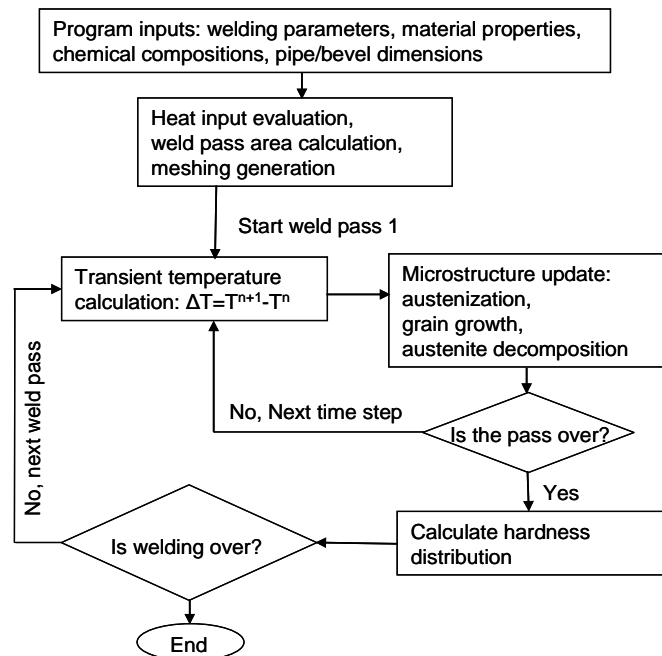


Figure 12. Flow diagram of thermal simulation for GMAW girth weld.

Finally, the thermal analysis software has a Microsoft Windows[®] interface for the execution of the simulation. Figure 13 shows the appearance of the interface. The input file must be prepared according to the required format before the simulation. The execution of simulation starts upon the clicking of the command “Girth Weld Analysis” under the Windows menu “Analysis”. All the output data are written in Microsoft Excel files, so data post-processing can be readily started.

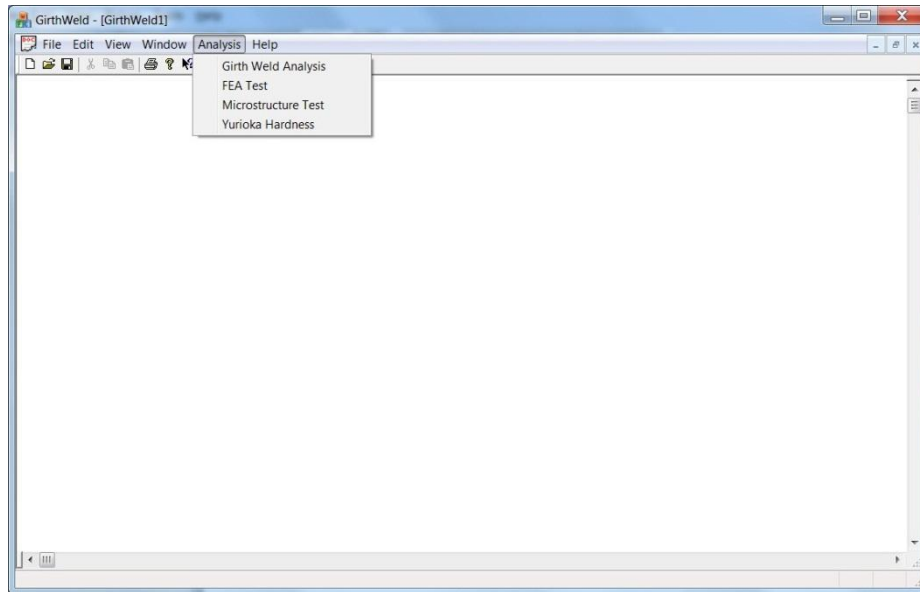


Figure 13. Microsoft Windows® interface of the thermal analysis software.

4 Verification and Applications of Thermal Model

The previous sections have described the technical approach for the thermal analysis procedure for the multi-pass, multi-wire GMAW girth welds. The procedure was implemented in two different formats. The first one was through the use of commercial finite element package ABAQUS. After the verification of the procedure with ABAQUS was complete and the procedure proved to be effective, the analysis procedure was automated through an implementation of finite element method.

In the process of development and implementations of the thermal analysis procedures, a number of sets of experimental data were used to calibrate and verify the procedure. The major data sets include:

- 1) The thermal cycle measurement data by Hudson^[10];
- 2) The thermal cycle measurement data from the first round girth welds;
- 3) The thermal cycle measurement data from the second round girth welds;
- 4) The thermal cycle measurement data from the third round girth welds;

The first attempt of model development and verification were very successful and established a solid foundation for later development. Furthermore, later implementations, verifications, and application of the model provided incremental improvements to the thermal model. These improvements will be clearly demonstrated in the results presented in the subsections below.

In addition to its verification, the implemented analysis procedure was also applied to the project research works as it was intended on several topics. These applications include:

- 1) Virtual experiments to assist identifying the welding essential variables;
- 2) Thermal simulations for dual torch GMAW to assist weld procedure designs;
- 3) Cooling rate calculations for dual torch GMAW to provide information for Gleeble simulation design;

In the following subsections, the verifications of this thermal analysis procedure and its applications are presented.

4.1 Verification of Thermal Analysis Procedure with Hudson's Thermal Data

This subsection presents the first implementation of the thermal analysis procedure, and the simulation results of the thermal model.

4.1.1 Model Development

The thermal analysis procedure described in Section 3.1 was implemented first with finite element software ABAQUS. The partitions of the girth welds, the parameters in the heat flux formulation were calculated prior to the construction of the model. The mesh was then generated over the partitioned girth weld, the HAZ, and the base metal. One of the meshes generated for this effort is shown in Figure 14.

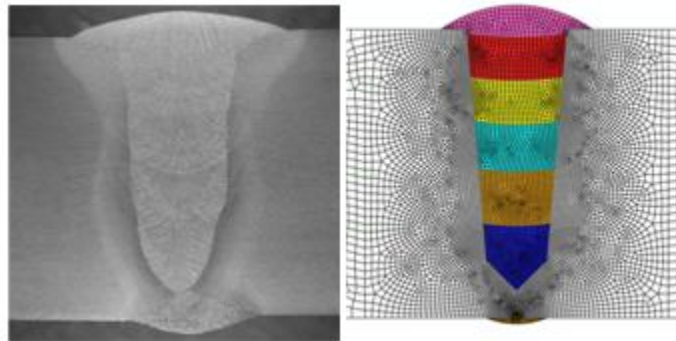


Figure 14. A multi-pass P-GMAW girth weld and its corresponding finite element mesh.

Cavity Radiation Effect

In the development of the thermal model, one additional factor considered was the cavity radiation at the bevel surfaces. The boundary condition in Eq. (3) applies to all the surfaces except the bevel surfaces. On these surfaces, because they are close to the hot weld metal and to each other, the so-called cavity radiation needs to be considered. This is illustrated in Figure 15, where the narrow opening of the groove results in a large portion of thermal radiation from the hot weld metal being captured by the bevel sidewalls. This captured thermal energy raises the sidewall temperatures at the bevel. The secondary radiations from the heated walls further transfer the thermal energy upwards. This cavity radiation enhances the heat transfer from the weld metal to its cold surroundings.

The heat flux formulation described by Equations (1) and (2) were implemented using ABAQUS user subroutines. For the cavity radiation, ABAQUS “*view factor” capability was used for the calculations of radiation heat flux. In addition, element removal and addition procedures were

followed to simulate the actual sequence of the multi-pass welding process. The thermal model also had inputs for temperature-dependent material properties such as thermal conductivity, specific heat, and latent heat for phase change effect.

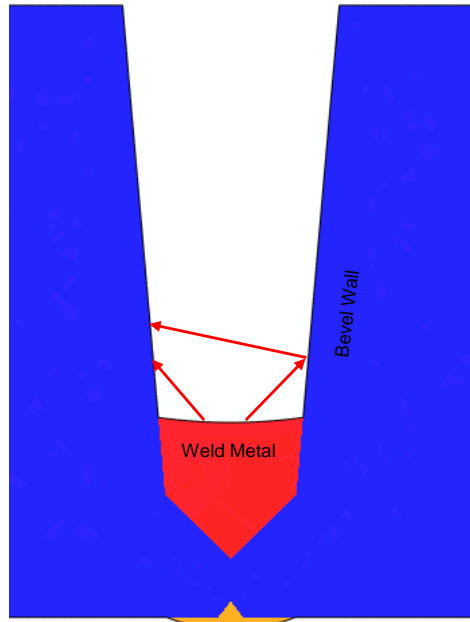


Figure 15. Cavity radiation in narrow groove P-GMAW.

4.1.2 Simulation Results

To verify the thermal model and numerical procedure described above, the experimental results of thermal cycle measurement data by Hudson^[10] were used.

The experimental measurements had two series data: (1) preheat variation trials and (2) process variation trials as they were called in the original work. The first series included measured thermal cycles under different pre-heat temperatures. The second series had measured thermal cycles with different P-GMAW variants, namely, single wire, tandem wire, and dual torch processes. Detailed information of the welding conditions for these girth welds can be found in Reference 10.

The first conclusion drawn from the thermal model was that the application of the cavity radiation did not lead to any significant difference in the thermal cycles. Consequently, this feature was eliminated from the model in all the model developments and simulations.

Simulation Results for Preheat Variation Trials

This set of data was obtained using single wire P-GMAW process with an internal root pass, one hot pass, and five fill passes. The pipes were X100 grade with a diameter of 752 mm (30 inches) and a wall thickness of 19.05 mm (0.75 inches). For these welding experiments three preheat temperatures were used: room temperature (27°C), 100°C, and 180°C. The pipes were preheated to the respective temperatures before the welding of each pass. Two groups of thermocouples

were used to monitor the thermal cycles in the weld metals. The first group were drilled and attached within each completed weld pass. The second group was plunged into the weld pool. Figure 16 shows a sketch of the single wire P-GMAW and the placement of the thermocouples. Because of the uncertainty in the actual locations of the plunged thermocouples, only the measurements from the first group of in-situ thermocouples were used in this work.

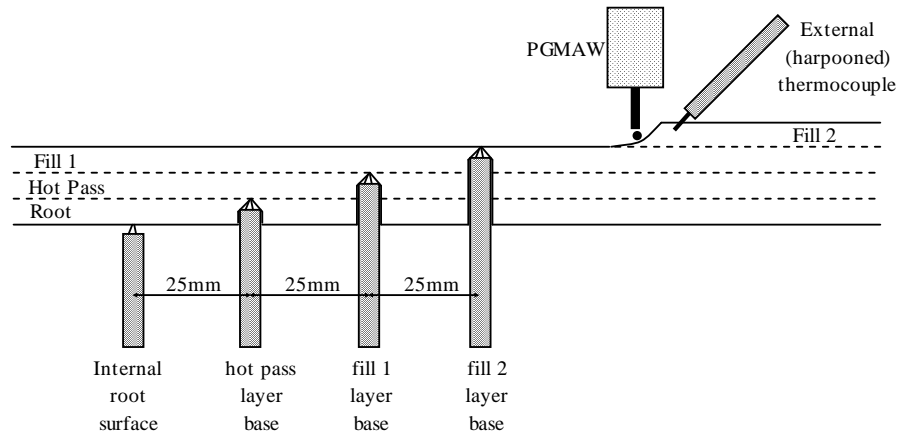


Figure 16. Cross-sectional view of single wire P-GMAW showing thermocouple placement.

As the single wire welding process progressed with each weld pass, thermocouples were inserted in holes drilled into the previously completed weld pass prior to deposition of the next pass. The thermal cycles were recorded utilizing each group of thermocouples. The cooling times from 800°C to 500°C, T_{85} , from 800°C to 400°C, T_{84} , from 800°C to 300°C, T_{83} , were calculated from the temperature histories.

Table 1 lists the measured (M) and predicted (P) cooling times for the different preheat conditions. It should be noted that pre-heat and inter-pass temperatures were maintained at the same-targeted values throughout welding. As expected there was a trend towards longer cooling times with increasing pre-heat/inter-pass temperatures, which was particularly evident for the T_{84} and T_{83} cooling times.

Table 1. Measured (M) and Predicted (P) Cooling Times for the preheat trials.

Preheat Temperature	Pass	T ₈₅ (s)			T ₈₄ (s)			T ₈₃ (s)		
		M	P	P/M	M	P	P/M	M	P	P/M
No Preheat	Hot Pass	3.4	3.2	0.9	5.9	5.2	0.9	9.1	8.5	0.9
	Fill 1	2.4	2.3	1.0	4.6	4.2	0.9	8.0	7.8	1.0
	Fill 2	2.4	2.5	1.1	4.4	4.5	1.0	7.8	9.4	1.2
	Fill 3	2.6	3.1	1.2	4.4	5.3	1.2	7.3	8.7	1.2
	Fill 4	2.8	2.3	0.8	5.0	4.3	0.9	8.1	9.0	1.1
	Cap	3.3	3.0	0.9	5.6	5.4	1.0	8.7	11.7	1.3
100°C	Hot Pass	5.6	4.2	0.8	9.1	7.8	0.9	16.9	14.5	0.9
	Fill 1	3.4	2.5	0.7	6.7	4.8	0.7	12.7	10.8	0.9
	Fill 2	2.8	2.7	1.0	5.5	5.5	1.0	12.5	14.0	1.1
	Fill 3	2.5	3.7	1.5	5.0	5.2	1.0	10.0	13.5	1.4
	Fill 4	3.4	3.0	0.9	6.7	5.4	0.8	12.6	11.8	0.9
	Cap	4.5	3.0	0.7	7.6	4.8	0.6	13.9	10.9	0.8
180°C	Hot Pass	9.1	8.7	1.0	16.6	14.9	0.9	52.9	46.5	0.9
	Fill 1	5.6	3.8	0.7	10.9	8.4	0.8	28.9	27.3	0.9
	Fill 2	4.3	4.4	1.0	9.8	10.8	1.1	29.2	28.0	1.0
	Fill 3	3.7	4.0	1.1	8.5	9.0	1.1	25.3	25.3	1.0
	Fill 4	4.3	4.4	1.0	8.7	9.3	1.1	21.9	28.7	1.3
	Cap	5.6	3.9	0.7	9.7	8.5	0.9	22.6	27.5	1.2
Statistical Measure of the Comparison		Median	0.95		Median	0.90		Median	0.99	
		Std. Dev.	0.20		Std. Dev.	0.14		Std. Dev.	0.18	

Figure 17 is the cumulative plot that shows the comparisons between the measured T₈₅ and those predicted by the thermal model. The T₈₅ values are close together and sometimes overlap at short times. Similarly, Figure 18 and Figure 19 show the comparisons of T₈₄ and T₈₃ between the measured and the predicted by the thermal model. They in general are in good agreement with a few points having relatively large differences (points on the x=y line present a perfect agreement). For cooling time T₈₃, the calculated results are quite sensitive to the values of convective heat transfer coefficient at the boundary.

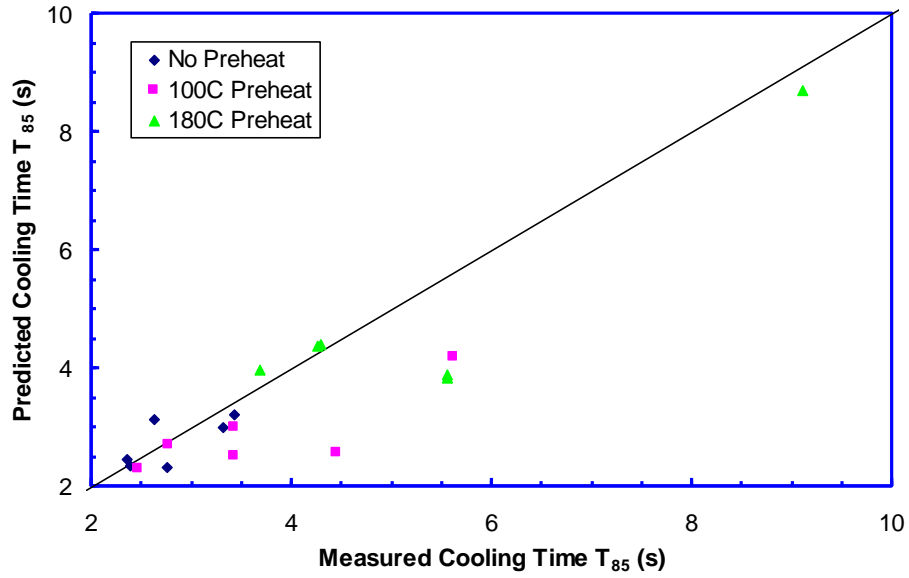


Figure 17. Comparisons of cooling time T_{85} between measurements and prediction for single-wire P-GMAW with different preheat temperatures.

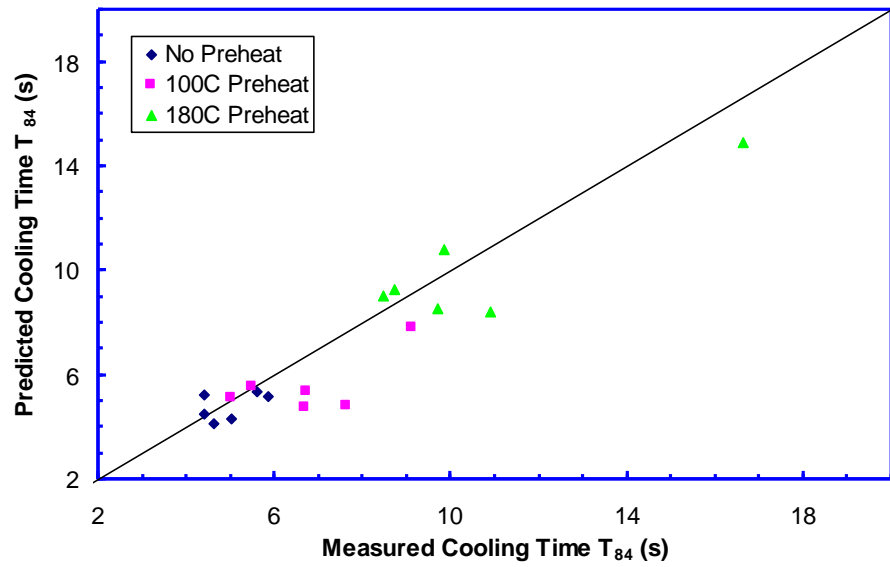


Figure 18. Comparisons of cooling time T_{84} between measurements and prediction for single wire P-GMAW with different preheat temperatures.

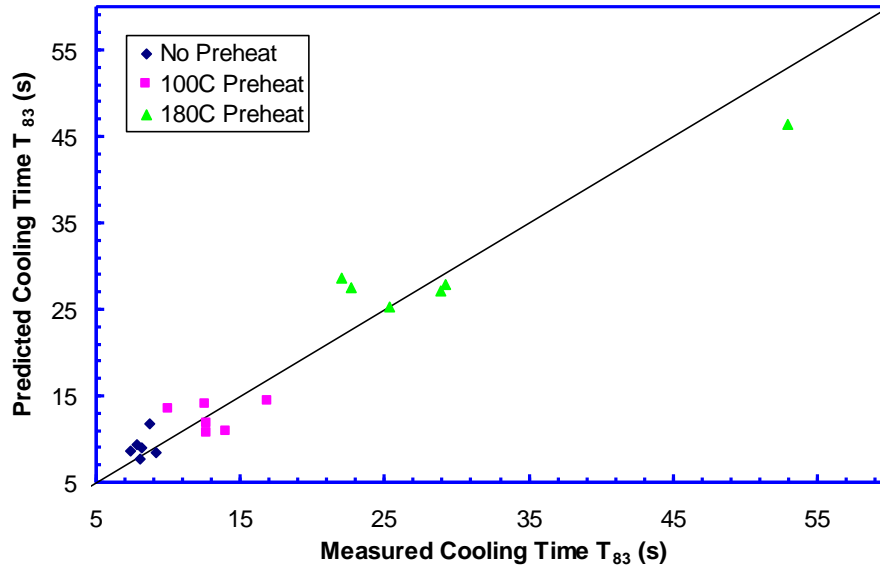


Figure 19. Comparisons of cooling time T_{83} between measurements and prediction for single wire P-GMAW with different preheat temperatures.

The discrepancies on the cooling times are partly attributable to the differences in weld geometries and heat input between the actual welding process and the thermal model. The transient response of the thermocouples is another subject worthy of further investigation. The thermocouples used in the measurements were 3.2 mm (1/8 inches) in diameter and the drilled holes were even larger. The rate of temperature change is quite high under the current welding conditions. The thermocouple reading could have reflected some degree of delay in heat transfer during the rapid thermal cycles.

Figure 20 shows the HAZ regions of the girth welds produced by the single torch GMAW with three pre-heat temperatures. The gray regions represent the molten area and the dark regions represent the base metal beyond the HAZ. It clearly shows from these contours that as the pre-heat temperature increases, the HAZ becomes wider.

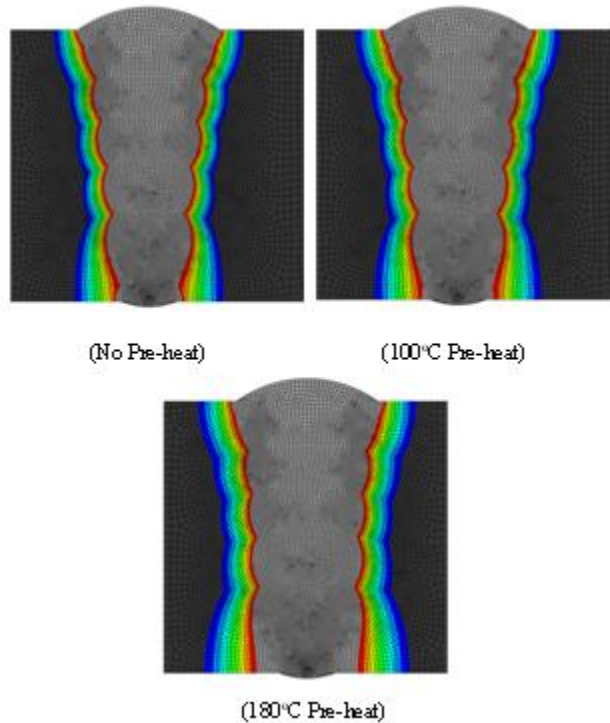


Figure 20. HAZ regions (colored) produced by single wire P-GMAW process under different pre-heat temperatures.

Simulation Results for Process Variation Trials

This part of verification of the thermal model focused on three different P-GMAW variants: single torch, tandem wire, and dual torch processes. For these experiments, the X100 grade pipes had a diameter of 914.4 mm (36 inches) and a wall thickness of 19.05mm (0.75 inches). All three processes used the same weld joint geometry design and all had the same pre-heat/inter-pass temperature of 100°C. The tandem wire consists of a single torch with two electrodes, arranged close together and feeding into the same weld pool (3.4 mm apart in this case). The dual torch process used two torches, each with a single wire and the wires were spaced 80 mm apart. Figure 21 shows the dual torch P-GMAW process and the placement of thermocouples underneath the passes.

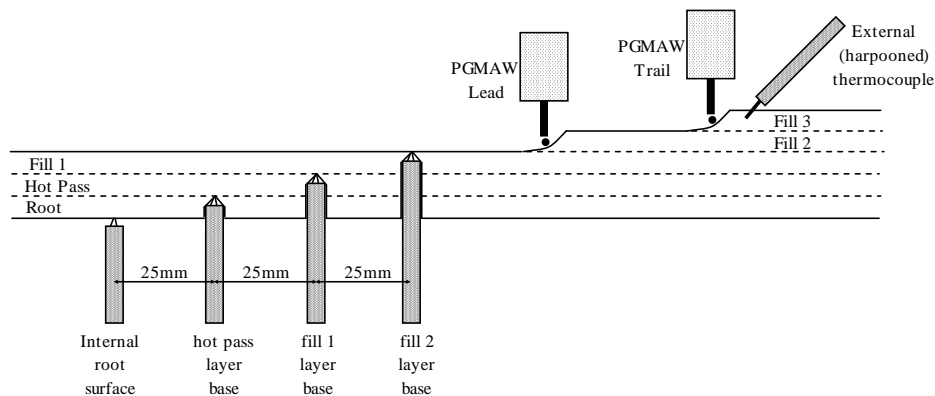


Figure 21. Sketch of dual torch GMAW process and thermocouple placements.

Figure 22 shows the finite element mesh used for this set of simulations.

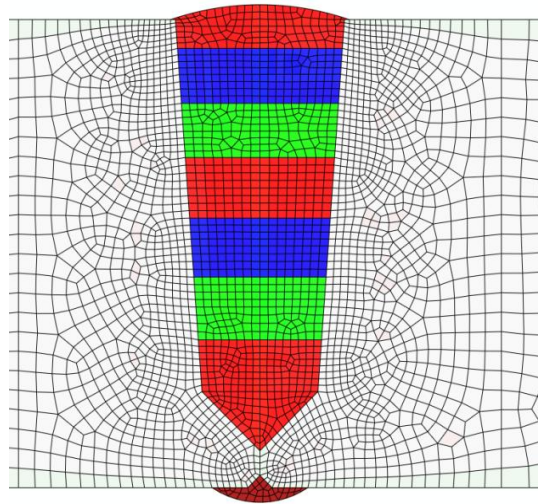


Figure 22. Finite element mesh for P-GMAW process variation trial. Colored weld regions represent weld metals deposited by different electrode wires.

Table 2 lists the measured (M) and predicted (P) cooling times for the three process variants. The missing measured data were due to the failures of thermocouples. In the dual torch case, measured T_{83} were not available. Figure 23, Figure 24, and Figure 25 are the cumulative plots that show the comparisons of measured and predicted cooling times with single wire, tandem wire, and dual torch. Good agreements are evident in cooling times T_{85} and T_{84} . However the simulated T_{83} times were consistently higher than the measured values. Given the good agreements in T_{85} and T_{84} times, the difference is apparently caused by the cooling times from 400°C to 300°C. Further investigation is under way to examine the differences.

Table 2. Measured and predicted cooling times for the process variation trials.

Process	Pass	T ₈₅ (s)			T ₈₄ (s)			T ₈₃ (s)					
		M	P	P/M	M	P	P/M	M	P	P/M			
Single Wire	Fill 1	2.9	3.0	1.0	4.2	5.9	1.4	12.4	12.7	1.0			
	Fill 2	2.1	2.1	1.0	4.5	4.6	1.0	9.9	11.2	1.1			
	Fill 3	1.9	2.1	1.1	4.0	4.6	1.2	7.9	12.2	1.6			
	Fill 4	2.0	2.2	1.1	4.1	4.5	1.1	8.0	11.4	1.4			
	Fill 5	2.3	2.1	0.9	4.7	4.3	0.9	8.7	11.1	1.3			
	Cap	3.1	2.4	0.8	5.7	4.7	0.8	9.9	11.0	1.1			
Tandem Wire	Fill 1	-	-	-	-	-	-	-	-	-			
	Fill 2	1.9	2.0	1.0	4.1	4.3	1.0	8.8	10.4	1.2			
	Fill 3	2.0	2.0	1.0	4.0	4.0	1.0	8.1	10.2	1.3			
	Fill 4	2.0	2.0	1.0	4.0	4.1	1.0	7.7	10.4	1.3			
	Fill 5	2.3	2.1	0.9	4.5	4.3	1.0	8.1	11.1	1.4			
	Cap	3.1	2.4	0.8	5.2	4.6	0.9	8.9	11.0	1.2			
Dual Torch	Fill 1	-	-	-	-	-	-	-	-	-			
	Fill 2	2.2	2.2	1.0	4.5	5.3	1.2	-	-	-			
	Fill 3	-	-	-	-	-	-	-	-	-			
	Fill 4	2.4	2.0	0.8	4.6	4.8	1.0	-	-	-			
	Fill 5	-	-	-	-	-	-	-	-	-			
	Cap	3.1	2.3	0.7	5.8	4.6	0.8	-	-	-			
Statistical Measure of the Comparison		Median	1.00			Median	1.02			Median	1.26		
		Std. Dev.	0.12			Std. Dev.	0.16			Std. Dev.	0.15		

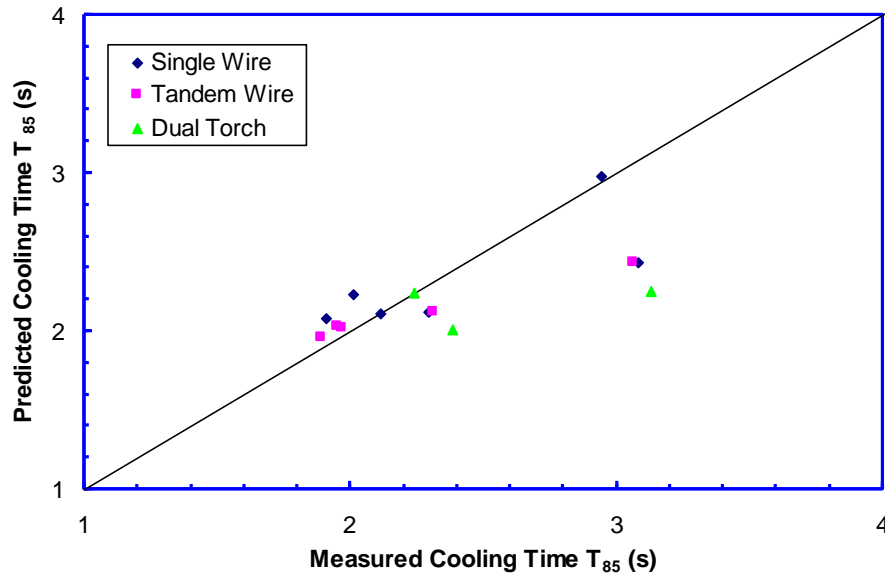


Figure 23. Comparisons of cooling time T₈₅ between measurements and prediction for different GMAW processes.

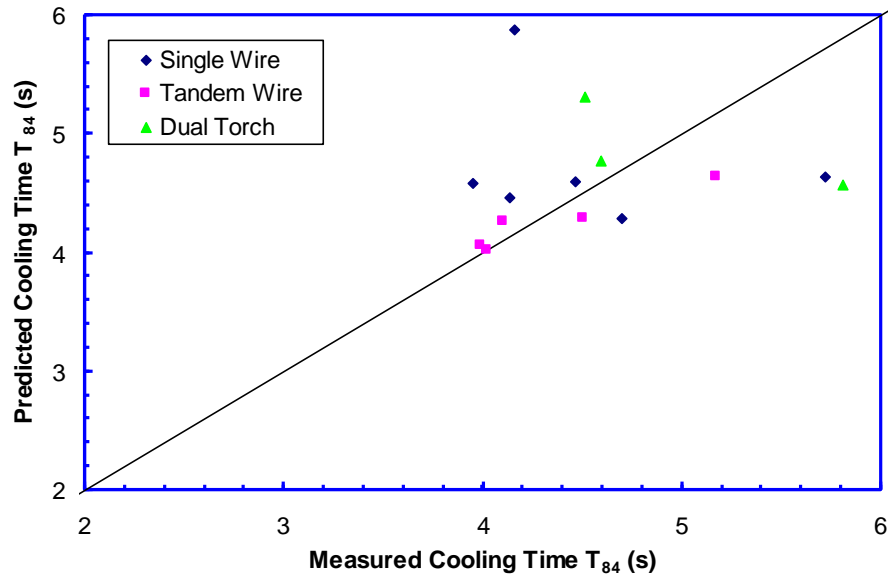


Figure 24. Comparisons of cooling time T_{84} between measurements and prediction for different GMAW processes.

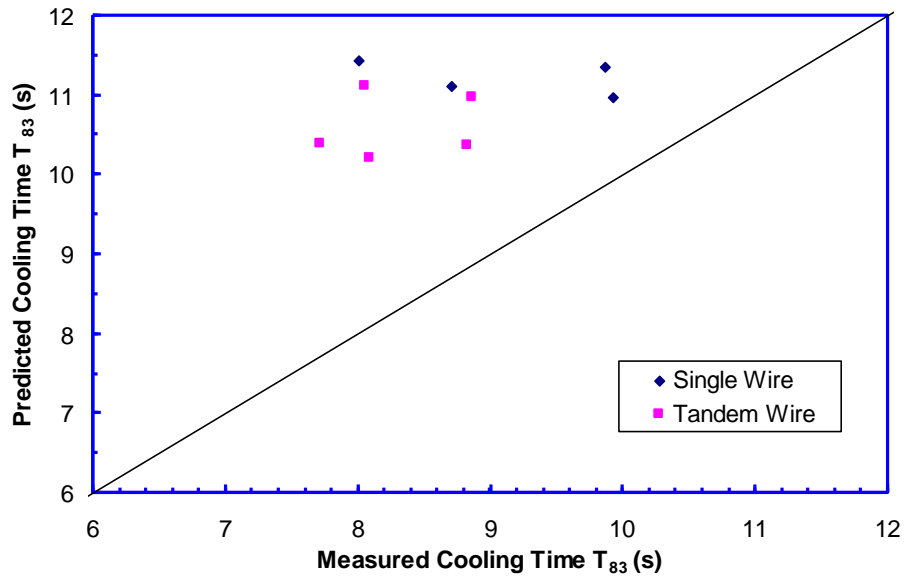


Figure 25. Comparisons of cooling time T_{83} between measurements and prediction for different GMAW processes.

Figure 26 shows the HAZ regions produced by the three GMAW processes. While the HAZ regions made by the single wire and the tandem wire processes have similar widths, the HAZ made by the dual torch process is much wider.

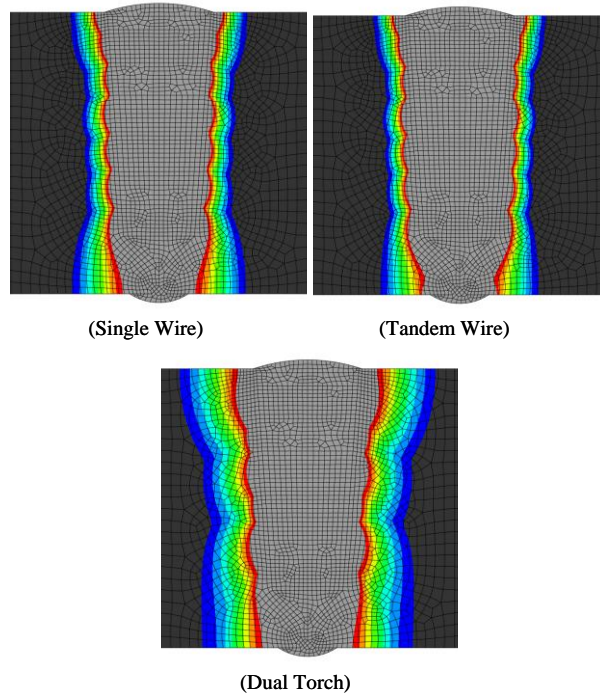


Figure 26. HAZ regions (colored) produced by single wire, tandem wire, and dual torch processes.

Thermal Cycles in Dual Torch GMAW

One of the major observations among different welding processes is that the dual torch process often produced a softer weld and HAZ. As pointed out by Hudson ^[10], this softened weld metal and HAZ were due to the longer cooling times during the dual torch welding. To illustrate the thermal cycles in this process, we picked two points in the weld metal to examine the thermal cycles at these locations. The two locations are shown in Figure 27. The thermal cycles at these two locations are plotted in Figure 28. It is observed that the lower location experiences two heating-cooling cycles as the dual torch passes through. The first one is due to the leading torch, and the second one is due to the trailing torch. The upper location, however, only experiences a single heating-cooling cycle.

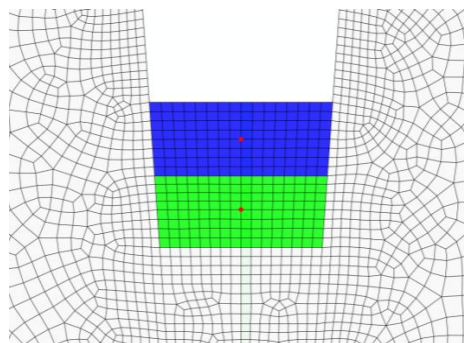


Figure 27. Two locations in the weld metals deposited by the dual torch in one pass. Green is by the leading torch, blue is by the trailing torch.

Furthermore, by examining the thermal cycles, it shows that the cooling time from the trailing torch is nearly twice of that from the leading torch. The reason that the cooling time for the

trailing torch is longer can be explained by examining the temperature field right before the trailing torch arrives.

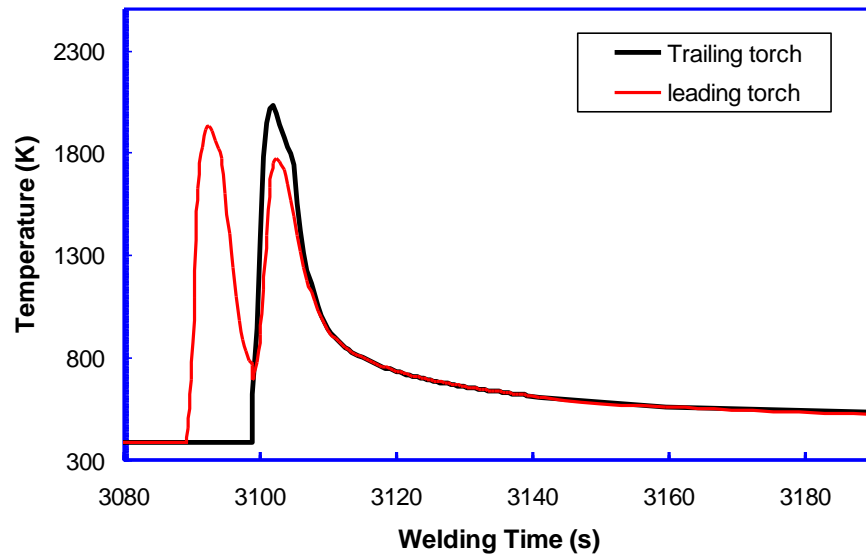


Figure 28. Thermal cycles experienced by two locations shown in Figure 27 during dual torch welding.

Figure 29 is the temperature contour right before the trailing torch arrives. This temperature field is the residual left behind by the leading torch. For the trailing torch, this “residual” temperature serves as a distributed “preheat” temperature. As can be seen in the contour, the temperature is still as high as 900K when the trailing torch arrives. This rather high “preheat” temperature, according to the analysis for the preheat trial results, certainly will lead to longer cooling times. This observation suggests that for the dual torch process, the combination of the heat inputs, the distance between the two torches, and the travel speed of the torches will play a critical role in determining the final properties of the weld.

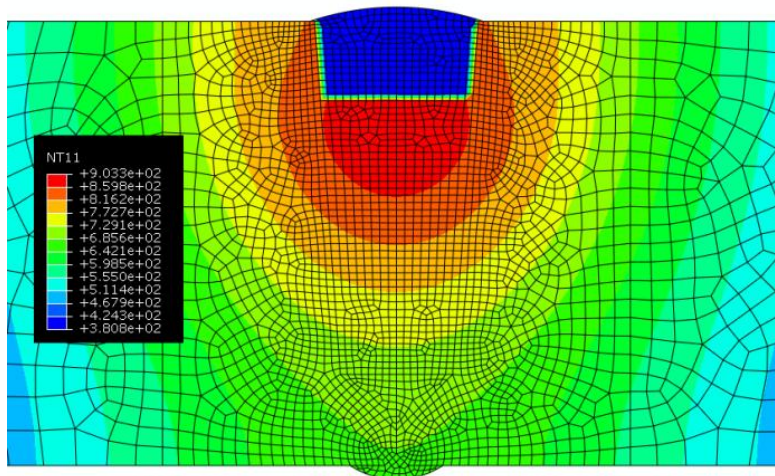


Figure 29. Temperature contour after the leading torch and right before the trailing torch for dual torch GMAW process.

4.2 Verification of Thermal Model with First Round Girth Welds

All of the first round girth welds were made with single torch P-GMAW^[20]. Two of the welds, tagged as 807J and 807K respectively, were instrumented for HAZ temperature measurements. Grounded K type thermocouples enclosed in a stainless sheath were used for the temperature measurement. A series of 1.6 mm (1/16-inch) holes were drilled at a 45 degree angle from inside surface of the pipe into the weld HAZ region. The thermocouples were inserted into the holes and connected to a National Instruments 32-channel Isothermal Terminal Block for data acquisition. Figure 30 shows one of the thermocouple locations for girth weld 807K.

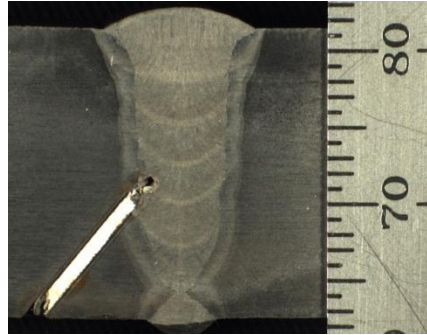


Figure 30. Section view of HAZ thermocouple in first round girth weld 807K. White region indicates the drilled hole for thermocouple.

Because of the delicate nature of thermocouple installation, not all thermocouples yielded useful data due to, for example, loss of contact or severe burn when the local temperature was too high. The temperature measurements from 807J were selected to compare with the predictions by the thermal model.

Weld 807J was made with single torch P-GMAW at 1G position during first round welding. The detailed welding conditions are listed in Table 3.

Table 3. Welding conditions for weld 807J.

Pass No.	Welding Current (A)	Welding Voltage (V)	Wire Feed Speed (m/min)	Travel Speed (mm/min)	Avg. Heat Input (kJ/mm)	True Heat Input (kJ/mm)	Heat Input Difference
Hot Pass	199.3	20.6	10.6	1342.0	0.209	0.242	16.0%
Fill Pass 1	199.6	22.0	10.6	505.7	0.589	0.682	15.8%
Fill Pass 2	198.8	22.5	10.6	505.6	0.595	0.676	13.6%
Fill Pass 3	198.7	22.4	10.6	505.7	0.589	0.683	15.8%
Fill Pass 4	198.4	22.5	10.6	505.8	0.587	0.683	16.4%
Fill Pass 5	198.4	22.5	10.6	455.4	0.648	0.758	16.9%
Cap Pass	147.6	23.5	8.2	445.2	0.505	0.617	22.2%

One observation from the table is that the true heat inputs for the waveform used during the girth welding were determined to be about 14-22% higher than the “averaged” heat inputs. This was also confirmed by the thermal model. A consistent result from the thermal model was that if the “averaged” heat inputs were used for a P-GMAW, the peak temperatures of thermal cycles were always under-predicted.

4.2.1 Thermal Cycle Comparison

One of the thermocouples instrumented in the weld is shown in Figure 31. It is clear from the figure that the thermocouple was placed to target the thermal cycles in the HAZ near the 5th fill pass.

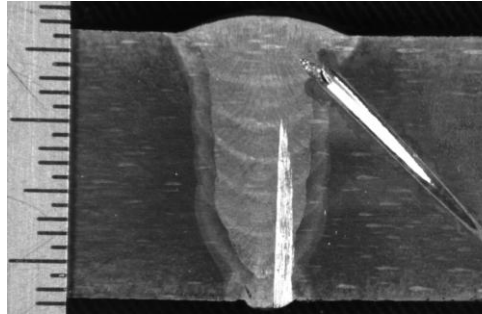


Figure 31. Location of thermocouple (F5A) for the temperature measurements for weld 807J.

The measured thermal cycles by the thermocouple shown in Figure 31 are plotted against the predictions by the thermal model in Figure 32. The agreement is excellent. One observation by examining the welding parameters listed in Table 3 is that the heat inputs varies from 0.18 kJ/mm to about 0.6 kJ/mm among the welding passes. This fact demonstrates the excellent robustness of the thermal model in dealing with large range of welding conditions.

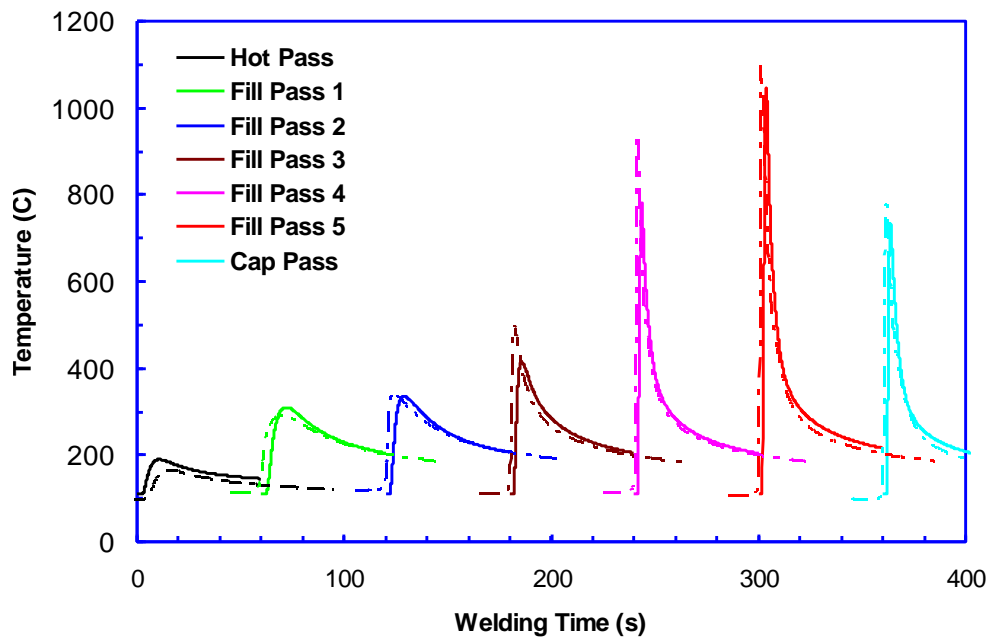


Figure 32. Comparison of measured and predicted thermal cycles at location shown in Figure 31. Curves with solid lines are by model prediction and dashed lines by thermocouple measurements.

4.2.2 Impact of True Heat Input

For the same weld 807J, another thermocouple (F2A) was placed in the HAZ targeting fill pass 2, as shown at the left of Figure 33. From the post-welding macrographs, the thermocouple is

actually seen at the junction of fill pass 1 and fill pass 2. For the thermal model, the partition of the welding passes and the temperature monitoring location are shown at the right of the same figure.

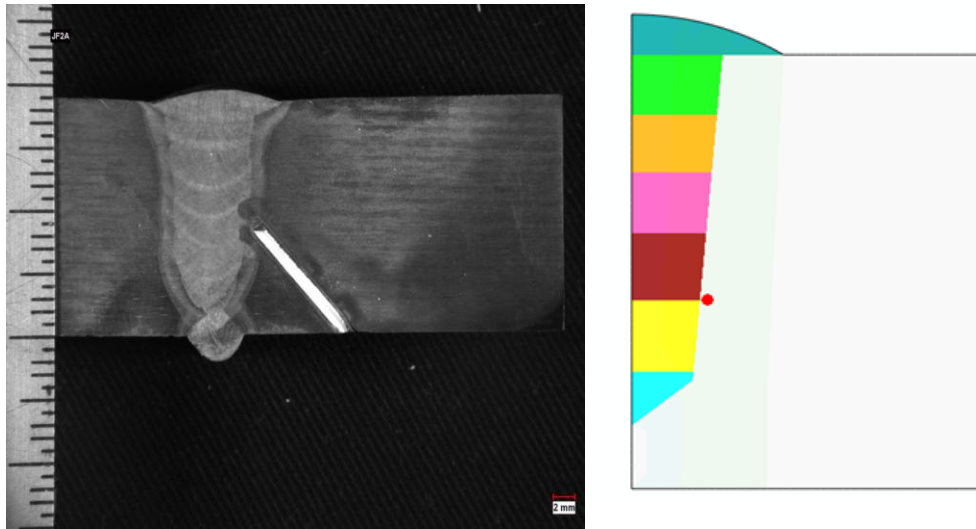


Figure 33. HAZ Thermocouple (F2A) location targeting fill pass 2 (right) and partition of girth weld by the thermal model. Red dot indicates the monitoring location for thermal cycles in the model.

In order to examine the impact of true heat input on thermal cycles, the “averaged” heat input and the true heat inputs in Table 3 were used for the predictions of thermal cycles. The computed thermal cycles for fill pass 1 and fill pass 2 were plotted against the measured thermal cycles by thermocouple F2A in Figure 34 and Figure 35, respectively.

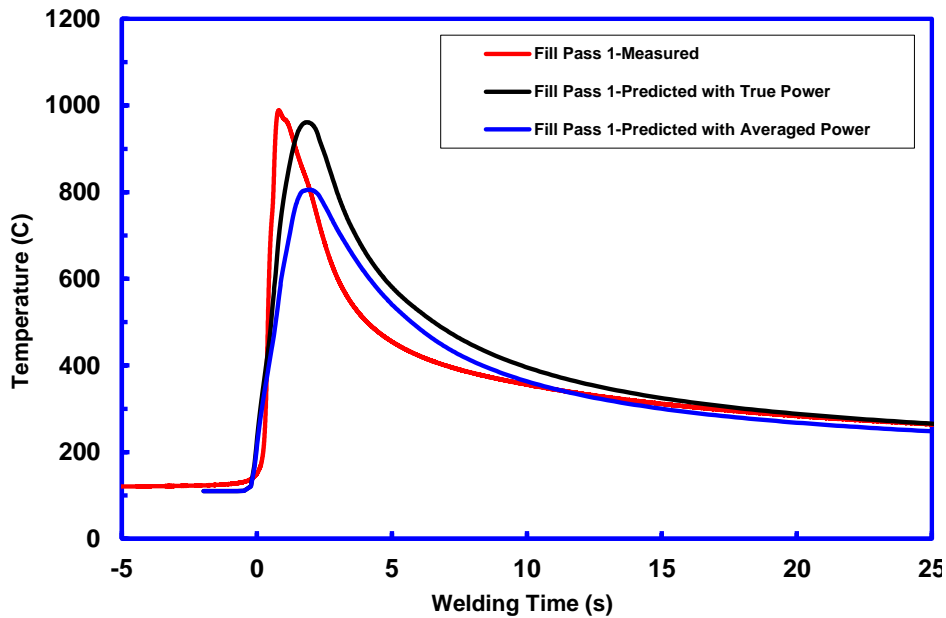


Figure 34. Comparison between measured thermal cycle for fill pass 1 and predicted thermal cycles with “averaged” heat inputs and true heat inputs.

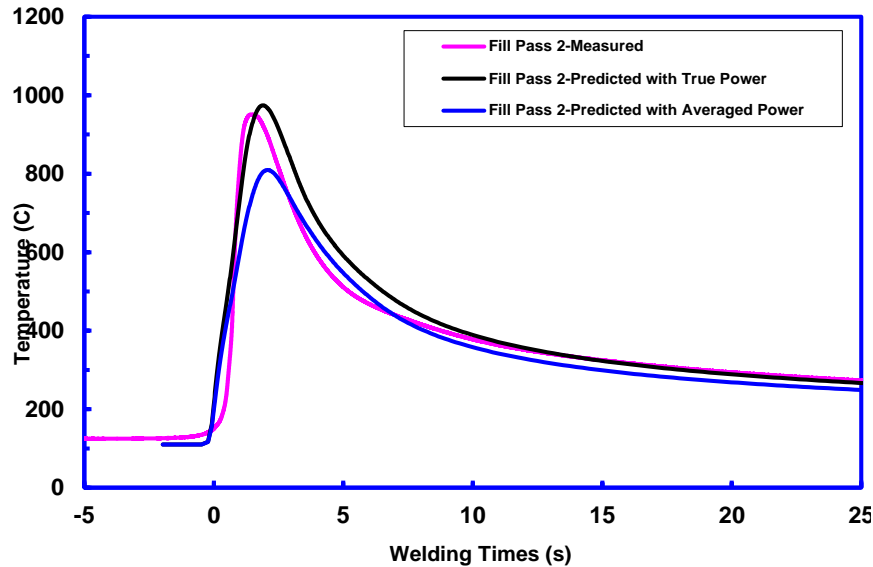


Figure 35. Comparison between measured thermal cycle for fill pass 2 and predicted thermal cycles with “averaged” heat inputs and true heat inputs.

From these plots, it is obvious that the simulations with “averaged” heat inputs under-predicted the peak temperatures of welding thermal cycles. One conclusion drawn from this result is that for P-GMAW, the conventional “averaged” heat input can be misleading when it is used for the evaluation of thermal cycles. In practice, when information on true heat input is not available, estimated compensation must be made to thermal cycle evaluation.

4.3 Verification of Thermal Model with Second Round Girth Welds

The second round girth welds were made with single torch P-GMAW and dual torch P-GMAW processes, and in 1G and 5G positions^[20]. To measure the temperature in the weld HAZ, thermocouples were made from bulk K-type thermocouple wire and 1.6 mm (1/16-inch) diameter ceramic insulating sleeves. Thermocouple wires were passed through a 7.94 mm (5/16-inch) length of heat shrink tubing and through the insulating sleeve. The wires were joined at the pointed end using a Rofin-Bassel Laser welder. Afterwards, holes of 1.69 mm (0.067 inch) in diameter were drilled at the internal surface of the pipe to accept the ceramic insulators. The orientation and depth of the holes were controlled to place the thermocouples in the desired HAZ locations. Finally, thermocouples were secured in the holes with a capacitor discharge welder to ensure contact with the pipe.

Individual pairs of 0.85 mm (0.03-inch) S-type thermocouple wires with ceramic insulating sleeves were used for measuring the temperature histories inside the weld metal. During welding, these thermocouples were plunged manually into the weld pool immediately behind the arc.

Among the girth welds made during the second round welding, the measured thermal cycles of two girth welds, 883J and 883H, were used for the comparisons with predicted results by the thermal model.

4.3.1 Girth Weld 883J

This weld was made with single torch P-GMAW in the 1G position during the second round welding. The key welding conditions are listed in Table 4.

Table 4. Welding conditions for weld 883J.

Pass No.	Welding Current (A)	Welding Voltage (V)	Wire Feed Speed (m/min)	Travel Speed (mm/min)	Heat Input (kJ/mm)
Hot Pass	224.5	23.1	12.6	594.4	0.52
Fill Pass 1	200.5	21.9	10.4	552.0	0.48
Fill Pass 2	200.5	21.9	10.4	552.0	0.48
Fill Pass 3	200.5	21.9	10.4	552.0	0.48
Fill Pass 4	200.5	21.9	10.4	552.0	0.48
Fill Pass 5	202.5	21.0	10.4	510.5	0.50
Cap Pass	146.5	22.8	7.1	461.0	0.43

As this weld was being made, thermocouples were plunged into the weld pool for each pass. With the exception of fill pass 2, all the plunged thermocouples recorded good temperature histories in the weld metal. These thermal cycles are plotted in Figure 36. The S-type thermocouple wires have a design peak temperature of 1450°C. Although the weld pool temperature exceeded this temperature limit when the thermocouples were plunged, the thermocouples were still able to survive because of the short duration at high temperature and recover their measuring capacities once the weld metal temperature is below 1450°C. These observations were clearly supported by the recorded thermal cycles in Figure 36.

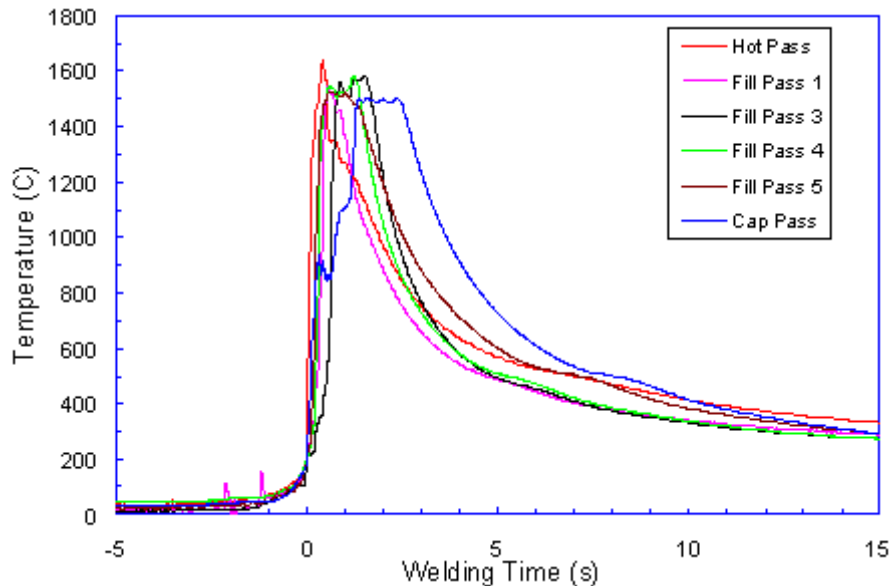


Figure 36. Measured thermal cycles from plunged thermocouples for weld 883J.

Again, the thermal model performed the welding simulation under the conditions listed in Table 4. The predicted thermal cycles from the weld metal during each pass were recorded and the cooling times T_{85} and T_{84} were determined. These predicted cooling times and those from the measured thermal cycles as in Figure 36 are listed in Table 5. The excellent agreement between

the measured cooling times and those predicted by the thermal model provides further support to the new methodology for heat flux application in the model.

Table 5. Comparison of measured and predicted cooling times T_{85} and T_{84} for weld 883J.

Pass	Hot Pass	Fill Pass 1	Fill Pass 3	Fill Pass 4	Fill Pass 5	Cap Pass	
T_{85} (s)	Measured	4.30	2.40	2.07	2.00	2.56	3.49
	Predicted	3.98	2.23	2.00	1.96	2.00	3.10
	Error (%)	7.4	7.1	3.2	2.0	21.9	11.2
T_{84} (s)	Measured	7.89	4.81	4.00	4.36	4.83	5.82
	Predicted	6.91	5.06	4.24	3.96	4.00	6.00
	Error (%)	12.4	5.1	6.1	9.2	17.2	3.1

4.3.2 Girth Weld 883H

This girth weld was made using a dual torch welding process in the fixed (5G) position in the second round welding. The key welding conditions for this dual torch weld are listed in Table 6.

Table 6. Welding conditions for dual-torch weld 883H.

Pass No.	Welding Current (A)	Welding Voltage (V)	Wire Feed Speed (m/min)	Travel Speed (mm/min)	Heat Input (KJ/mm)
Hot Pass	237.5	23.0	12.7	593.0	0.53
Pass 1 (lead)	197.0	22.0	10.0	491.0	0.50
Pass 1 (trail)	197.0	22.0	10.0	491.0	0.50
Pass 2 (lead)	197.0	22.0	10.0	491.0	0.50
Pass 2 (trail)	197.0	22.0	10.0	491.0	0.50
Fill Pass 3	186.5	22.0	10.0	481.3	0.56
Cap Pass	142.0	23.8	6.7	416.6	0.56

The thermal cycles in the HAZ near the hot pass was recorded by a thermocouple. They are plotted in Figure 37. The predicted thermal cycles at the same location as the thermocouple are also plotted in the same figure. The agreement between the measured and the predicted thermal cycles is reasonably good. The thermal model is not only able to capture the peak temperatures as welding passes with different torch settings are applied, it also correctly follows the time delays between the leading and trailing torches. This result is a solid proof that the combination of the new heat flux model and the superimposition principle works very well for the simulation of dual torch welding.

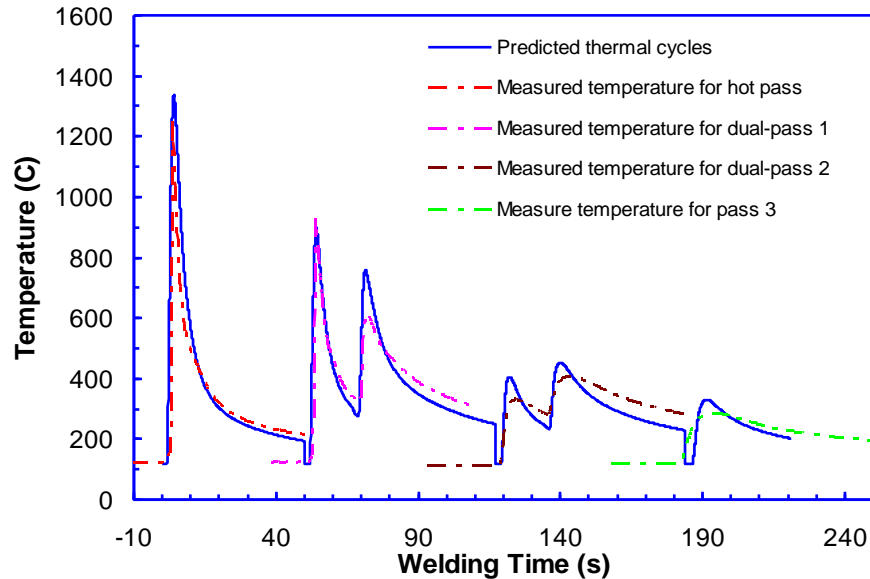


Figure 37. Measured and predicted thermal cycles in HAZ of girth weld made with dual torch P-GMAW.

4.4 Virtual Experiments and Identification of Essential Variables

The essential part of the project research work was a complete assessment of essential variables and improved understanding of the factors influencing properties of high strength steel pipeline girth welds and their performance.

After the thermal model (and the microstructure model) went through three rounds of calibrations and verifications against the measured thermal cycle data, i.e., the Hudson data, the data from the first round girth welds, and the data from the second round girth welds, it proved to be accurate in predicting thermal cycles for multi-pass, multi-wire GMAW and reasonably accurate in predicting the hardness. Subsequently, the thermal model was used as the primary tool to conduct a virtual experiment to identify the essential welding variables.

In this section, the design, execution, and results of the virtual experiment are presented. The microstructure-related results on hardness are also presented here for the purpose of data integrity.

The outputs of the virtual experiment were taken to perform a sensitivity study. This sensitivity study on the dependency of cooling times and weld metal hardness on the welding variables led to the identifications of welding essential variables. The process of this sensitivity study and its results are covered in a different topical report, Report 278-T-08^[14].

4.4.1 Virtual Experiment Matrix

The baseline case for the virtual experiments was based on the first and second rounds girth welds. In developing the virtual experiment matrix, the following parameters and their values were shared by all the tests (see Figure 4 for bevel-related dimensions):

- 1) Pipe outer diameter: 914.4 mm (36 inches)
- 2) Pipe wall thickness: 19.05 mm (0.75 inches)
- 3) Bevel angle: 5°
- 4) Bevel offset angle: 52°
- 5) Bevel land depth: 1.0 mm
- 6) Internal bevel depth: 0.5 mm
- 7) Internal bevel angle: 37.5°
- 8) Torch distance: 101.6 mm for dual torch only

The experiment matrix was developed by changing the following welding parameters:

- 1) Bevel offset
- 2) Pre-heat/inter-pass temperature
- 3) Torch configuration
- 4) Welding procedure
- 5) Electrode type

The total matrix of the virtual experiment is listed in Table 7. The bevel offset values included 0.09 and 0.11 inches. The pre-heat and inter-pass temperatures were kept the same value for each weld. In the matrix, three levels were used: 27°C, 100°C, and 180°C. The torch configuration included single and dual torches. Three electrode types were considered in the experiments: a NiMo type, Prototype 1, and Prototype 2.

Another variable in the matrix is the welding procedure. In total, 8 (A-H) welding procedures were considered. The detailed welding conditions of these procedures are listed in Tables 8 through 15.

Table 7. Virtual Experiment Matrix

Run No.	Bevel Offset	Pre-heat / Inter-pass Temperature	Torch Configuration	Welding Procedure	Electrode
1	0.09	100C/100C	Single	A	NiMo
2	0.09	100C/100C	Single	B	NiMo
3	0.09	180C/180C	Single	A	NiMo
4	0.09	180C/180C	Single	B	NiMo
5	0.09	27C/27C	Single	A	NiMo
6	0.09	27C/27C	Single	B	NiMo
7	0.11	100C/100C	Single	C	NiMo
8	0.11	100C/100C	Single	D	NiMo
9	0.11	180C/180C	Single	C	NiMo
10	0.11	180C/180C	Single	D	NiMo
11	0.11	27C/27C	Single	C	NiMo
12	0.11	27C/27C	Single	D	NiMo
13	0.09	100C/100C	Dual	E	NiMo
14	0.09	100C/100C	Dual	F	NiMo
15	0.09	180C/180C	Dual	E	NiMo
16	0.09	180C/180C	Dual	F	NiMo
17	0.09	27C/27C	Dual	E	NiMo
18	0.09	27C/27C	Dual	F	NiMo
19	0.11	100C/100C	Dual	G	NiMo
20	0.11	100C/100C	Dual	H	NiMo
21	0.11	180C/180C	Dual	G	NiMo
22	0.11	180C/180C	Dual	H	NiMo
23	0.11	27C/27C	Dual	G	NiMo
24	0.11	27C/27C	Dual	H	NiMo
25	0.09	27C/27C	Single	A	PT1
26	0.09	180C/180C	Single	B	PT1
27	0.11	27C/27C	Single	C	PT1
28	0.11	180C/180C	Single	D	PT1
29	0.09	27C/27C	Dual	E	PT1
30	0.09	180C/180C	Dual	F	PT1
31	0.11	27C/27C	Dual	G	PT1
32	0.11	180C/180C	Dual	H	PT1
33	0.09	27C/27C	Single	A	PT2
34	0.09	180C/180C	Single	B	PT2
35	0.11	27C/27C	Single	C	PT2
36	0.11	180C/180C	Single	D	PT2
37	0.09	27C/27C	Dual	E	PT2
38	0.09	180C/180C	Dual	F	PT2
39	0.11	27C/27C	Dual	G	PT2
40	0.11	180C/180C	Dual	H	PT2

Notes: Bevel offset 2.3 mm (0.09 inches) and 2.8 mm (0.11 inches)

Table 8. Welding Procedure A.

Welding Procedure: A			Torch Configuration: Single			Torch Distance: N/A			
Pass No.	Voltage (V)	Current (A)	Travel Speed (ipm)	WFS (ipm)	Oscillation Frequency (Hz)	Oscillation Width (mm)	CTWD (mm)	Average Heat Input (kJ/in)	True Heat Input (kJ/in)
Root Pass	21	145	28	305	0	0	10	6.5	7.6
Hot Pass	21	140	22	286	0	0	19	8.0	9.4
FP1	21	140	22	286	3.33	4.1	16	8.0	9.4
FP2	21	140	22	286	3.33	4.4	13	8.0	9.4
FP3	21	140	22	286	3.33	4.7	13	8.0	9.4
FP4	21	140	22	286	3.33	5.0	13	8.0	9.4
FP5	21	140	22	286	3.33	5.3	13	8.0	9.4
FP6	21	140	22	286	3.33	5.6	13	8.0	9.4
FP7	21	140	22	286	3.33	5.9	13	8.0	9.4
FP8	21	140	22	286	3.33	6.1	13	8.0	9.4
Cap Pass	22.5	136	23	262	3.33	6.3	13	8.0	9.8

Table 9. Welding Procedure B.

Welding Procedure: B			Torch Configuration: Single			Torch Distance: N/A			
Pass No.	Voltage (V)	Current (A)	Travel Speed (ipm)	WFS (ipm)	Oscillation Frequency (Hz)	Oscillation Width (mm)	CTWD (mm)	Average Heat Input (kJ/in)	True Heat Input (kJ/in)
Root Pass	21	145	28	305	0	0	10	6.5	7.6
Hot Pass	22	194	17	408	0	0	19	15.1	17.6
FP1	22	194	17	408	3	4.1	16	15.1	17.6
FP2	22	194	17	408	3	4.4	13	15.1	17.6
FP3	22	194	17	408	3	4.7	13	15.1	17.6
FP4	22	194	17	408	3	5.0	13	15.1	17.6
Cap Pass	24	178	17	377	3	6.3	13	15.1	18.4

Table 10. Welding Procedure C.

Welding Procedure: C			Torch Configuration: Single			Torch Distance: N/A			
Pass No.	Voltage (V)	Current (A)	Travel Speed (ipm)	WFS (ipm)	Oscillation Frequency (Hz)	Oscillation Width (mm)	CTWD (mm)	Average Heat Input (kJ/in)	True Heat Input (kJ/in)
Root Pass	21	145	28	305	0	0	10	6.5	7.6
Hot Pass	21	140	22	286	0	0	19	8.0	9.4
FP1	21	140	22	286	3.33	5	16	8.0	9.4
FP2	21	140	22	286	3.33	5.3	13	8.0	9.4
FP3	21	140	22	286	3.33	5.6	13	8.0	9.4
FP4	21	140	22	286	3.33	5.9	13	8.0	9.4
FP5	21	140	22	286	3.33	6.2	13	8.0	9.4
FP6	21	140	22	286	3.33	6.5	13	8.0	9.4
FP7	21	140	22	286	3.33	6.7	13	8.0	9.4
FP8	21	140	22	286	3.33	6.9	13	8.0	9.4
FP9	21	140	22	286	3.33	7.2	13	8.0	9.4
Cap Pass	22.5	136	23	262	3.33	7.4	13	8.0	9.8

Table 11. Welding Procedure D.

Welding Procedure: D			Torch Configuration: Single			Torch Distance: N/A			
Pass No.	Voltage (V)	Current (A)	Travel Speed (ipm)	WFS (ipm)	Oscillation Frequency (Hz)	Oscillation Width (mm)	CTWD (mm)	Average Heat Input (kJ/in)	True Heat Input (kJ/in)
Root Pass	21	145	28	305	0	0	10	6.5	7.6
Hot Pass	22	194	17	408	0	0	19	15.1	17.6
FP1	22	194	17	408	3	5	16	15.1	17.6
FP2	22	194	17	408	3	5.3	13	15.1	17.6
FP3	22	194	17	408	3	5.6	13	15.1	17.6
FP4	22	194	17	408	3	5.9	13	15.1	17.6
Cap Pass	24	178	17	377	3	7.2	13	15.1	18.4

Table 12. Welding Procedure E.

Welding Procedure: E			Torch Configuration: Single			Torch Distance: N/A			
Pass No.	Voltage (V)	Current (A)	Travel Speed (ipm)	WFS (ipm)	Oscillation Frequency (Hz)	Oscillation Width (mm)	CTWD (mm)	Average Heat Input (kJ/in)	True Heat Input (kJ/in)
Root Pass	21	145	28	305	0	0	10	6.5	7.6
Hot Pass-LT	21	140	22	286	0	0	19	8.0	9.4
FP1-LT	21	140	22	286	3.33	4.1	16	8.0	9.4
FP2-TT	21	140	22	286	3.33	4.4	13	8.0	9.4
FP3-LT	21	140	22	286	3.33	4.7	13	8.0	9.4
FP4-TT	21	140	22	286	3.33	5.0	13	8.0	9.4
FP5-LT	21	140	22	286	3.33	5.3	13	8.0	9.4
FP6-TT	21	140	22	286	3.33	5.6	13	8.0	9.4
FP7-LT	21	140	22	286	3.33	5.9	13	8.0	9.4
FP8-TT	21	140	22	286	3.33	6.1	13	8.0	9.4
Cap Pass	22.5	136	23	262	3.33	6.3	13	8.0	9.8

Table 13. Welding Procedure F.

Welding Procedure: F			Torch Configuration: Dual			Torch Distance: 4 in.			
Pass No.	Voltage (V)	Current (A)	Travel Speed (ipm)	WFS (ipm)	Oscillation Frequency (Hz)	Oscillation Width (mm)	CTWD (mm)	Average Heat Input (kJ/in)	True Heat Input (kJ/in)
Root Pass	21	145	28	305	0	0	10	6.5	7.6
Hot Pass-LT	22	194	17	408	0	0	19	15.1	17.6
FP1-LT	22	194	17	408	3	4.1	16	15.1	17.6
FP2-TT	22	194	17	408	3	4.4	13	15.1	17.6
FP3-LT	22	194	17	408	3	4.7	13	15.1	17.6
FP4-TT	22	194	17	408	3	5.0	13	15.1	17.6
Cap Pass-LT	24	178	17	377	3	6.3	13	15.1	18.4

Table 14. Welding Procedure G.

Welding Procedure: G			Torch Configuration: Dual			Torch Distance: 4 in.			
Pass No.	Voltage (V)	Current (A)	Travel Speed (ipm)	WFS (ipm)	Oscillation Frequency (Hz)	Oscillation Width (mm)	CTWD (mm)	Average Heat Input (kJ/in)	True Heat Input (kJ/in)
Root Pass	21	145	28	305	0	0	10	6.5	7.6
Hot Pass-LT	21	140	22	286	0	0	16	8.0	9.4
FP1-LT	21	140	22	286	3.33	5	13	8.0	9.4
FP2-TT	21	140	22	286	3.33	5.3	13	8.0	9.4
FP3-LT	21	140	22	286	3.33	5.6	13	8.0	9.4
FP4-TT	21	140	22	286	3.33	5.9	13	8.0	9.4
FP5-LT	21	140	22	286	3.33	6.2	13	8.0	9.4
FP6-TT	21	140	22	286	3.33	6.5	13	8.0	9.4
FP7-LT	21	140	22	286	3.33	6.7	13	8.0	9.4
FP8-TT	21	140	22	286	3.33	6.9	13	8.0	9.4
FP9-LT	21	140	22	286	3.33	7.2	13	8.0	9.4
Cap Pass-LT	22.5	136	23	262	3.33	7.4	13	8.0	9.8

Table 15. Welding Procedure H.

Welding Procedure: H			Torch Configuration: Dual			Torch Distance: 4 in.			
Pass No.	Voltage (V)	Current (A)	Travel Speed (ipm)	WFS (ipm)	Oscillation Frequency (Hz)	Oscillation Width (mm)	CTWD (mm)	Average Heat Input (kJ/in)	True Heat Input (kJ/in)
Root Pass	21	145	28	305	0	0	10	6.5	7.6
Hot Pass-LT	22	194	17	408	0	0	19	15.1	17.6
FP1-LT	22	194	17	408	3	5	16	15.1	17.6
FP2-TT	22	194	17	408	3	5.3	13	15.1	17.6
FP3-LT	22	194	17	408	3	5.6	13	15.1	17.6
FP4-TT	22	194	17	408	3	5.9	13	15.1	17.6
Cap Pass-LT	24	178	17	377	3	7.2	13	15.1	18.4

4.4.2 Execution of Virtual Experiment

After the experiment matrix was finalized, 40 input files, one for each experiment case, were compiled according to the welding conditions specified in Tables 8 to 15.

The simulations of the 40 cases were executed on a 32-bit Microsoft Windows personal computer. A typical execution of one simulation was about 30 minutes, although actual calculation times for each case can be longer or shorter, depending on the total heat input of the case, and the total number of welding passes.

As stated before, the thermal analysis software outputs many simulation results by default. The information includes peak temperature and hardness snapshots of the whole domain at the end of each welding pass. For each pass, thermal cycles at three locations were output: the top surface of the pass, the middle point of the pass, and the HAZ of the pass. Two key pieces of information from the outputs were selected to represent the overall properties of the welding process and the weld. The first one is the cooling times T_{85} and T_{84} of the thermal cycle at the HAZ of fill pass 1; the second overall property is the hardness profile along the weld centerline and the hardness profile across the weld at the middle plane of the pipe.

4.4.3 Results from Virtual Experiment

To demonstrate the results from the virtual experiment, Figure 38 and Figure 39 plot the thermal cycles at the HAZ of fill pass 1 and the hardness profile along the weld centerline, respectively, for case 9, single torch welding procedure. Figure 40 and Figure 41 plot the same things for case 13, a dual torch welding procedure.

The cooling times T_{85} and T_{84} were calculated from the thermal cycles. For single torch processes, the thermal cycles are single cycles and the determinations are straight forward. For dual torch processes, however, there are situations when T_{85} , and especially T_{84} are not available. For instance, when the pre-heat temperature is high, heat input for the lead torch is high, or the torch distance is short, the temperature behind the lead torch may not be able to cool below 400°C or even 500°C before the trailing torch starts the heating.

Table 16 and Table 17 summarize the cooling times T_{85} and T_{84} for the single torch cases and the dual torch cases, respectively. The impacts of preheat temperature, torch configuration and welding heat inputs on the cooling times were quite obvious.

The microstructure data from the virtual experiment were used directly in the sensitivity study to identify the welding essential variables. The summary of the microstructure data and how they were used in the process are covered in a different topical report of the project, Report 278-T-08.

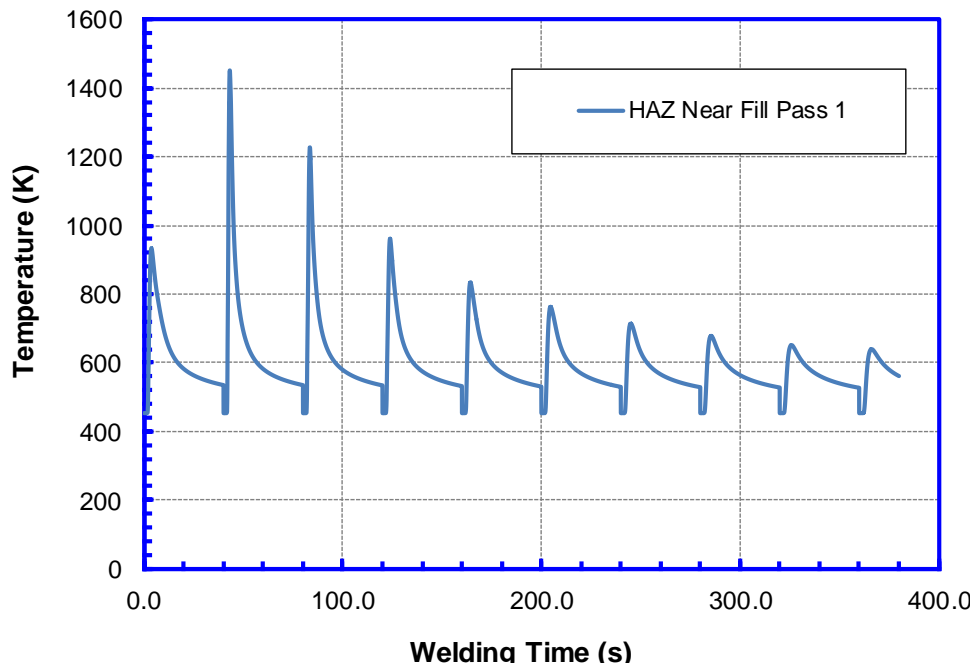


Figure 38. Simulated thermal cycles for case 9 of the virtual experiment.

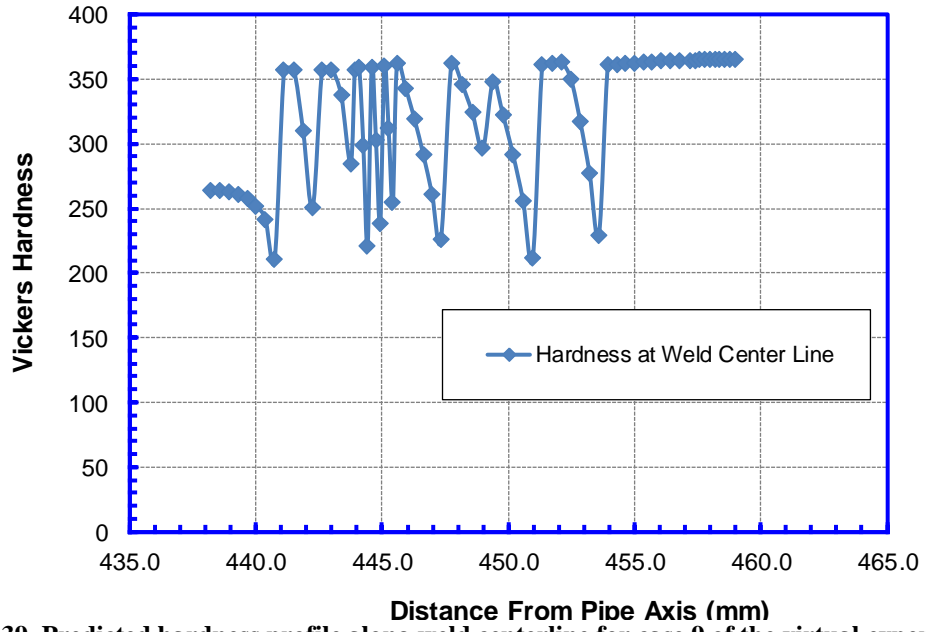


Figure 39. Predicted hardness profile along weld centerline for case 9 of the virtual experiment.

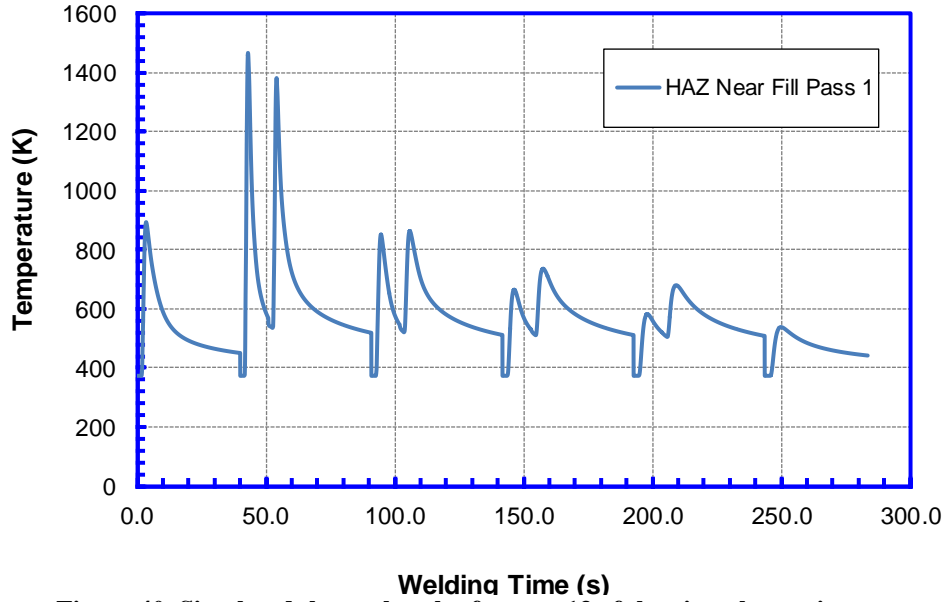


Figure 40. Simulated thermal cycles for case 13 of the virtual experiment.

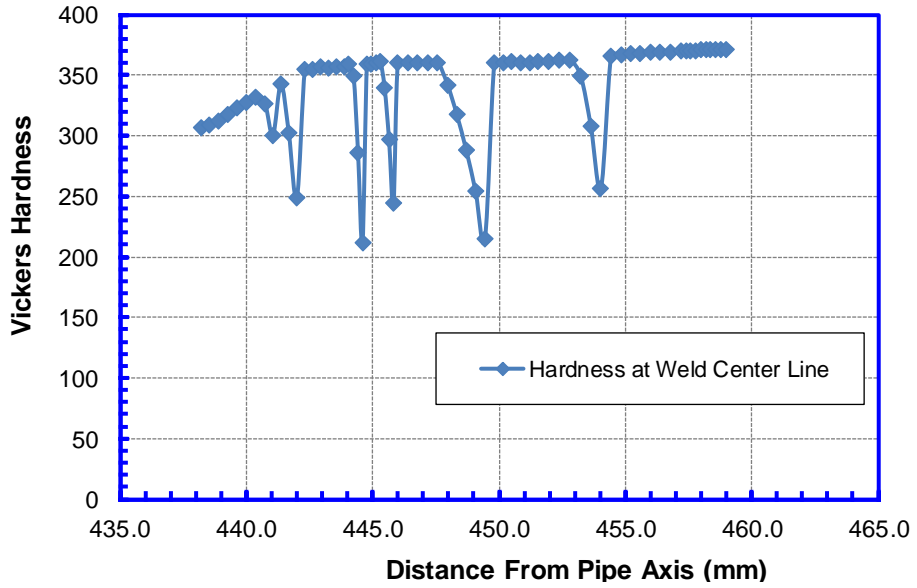


Figure 41. Predicted hardness profile along weld centerline for case 13 of the virtual experiment.

Table 16. Virtual Experiment: Summary of cooling times for single torch GMAW processes.

Run No.	Bevel Offset	Pre-heat / Inter-pass Temperature	Welding Procedure	Electrode	T ₈₅ at HAZ of FP1 (s)	T ₈₄ at HAZ of FP1 (s)
1	0.09	100C/100C	A	NiMo	1.71	3.06
2	0.09	100C/100C	B	NiMo	2.96	5.92
3	0.09	180C/180C	A	NiMo	2.51	5.34
4	0.09	180C/180C	B	NiMo	4.8	11.69
5	0.09	27C/27C	A	NiMo	1.34	2.12
6	0.09	27C/27C	B	NiMo	2.18	3.75
7	0.11	100C/100C	C	NiMo	1.96	3.54
8	0.11	100C/100C	D	NiMo	3.83	7.86
9	0.11	180C/180C	C	NiMo	2.91	6.08
10	0.11	180C/180C	D	NiMo	4.74	11.75
11	0.11	27C/27C	C	NiMo	1.48	2.43
12	0.11	27C/27C	D	NiMo	2.74	4.89
25	0.09	27C/27C	A	PT1	1.31	2.12
26	0.09	180C/180C	B	PT1	4.74	11.74
27	0.11	27C/27C	C	PT1	1.48	2.43
28	0.11	180C/180C	D	PT1	6.34	15.42
33	0.09	27C/27C	A	PT2	1.34	2.12
34	0.09	180C/180C	B	PT2	4.74	11.74
35	0.11	27C/27C	C	PT2	1.48	2.43
36	0.11	180C/180C	D	PT2	4.74	11.74

Table 17. Virtual Experiment: Summary of cooling times for dual-torch GMAW processes.

Run No.	Bevel Offset	Pre-heat / Inter-pass Temperature	Welding Procedure	Electrode	T ₈₅ at HAZ of FP1(s)		T ₈₄ at HAZ of FP1 (s)	
					Lead	Trail	Lead	Trail
13	0.09	100C/100C	E	NiMo	1.72	3.25	3.10	6.65
14	0.09	100C/100C	F	NiMo	2.96	8.82	5.92	20.87
15	0.09	180C/180C	E	NiMo	2.51	5.47	5.34	14.00
16	0.09	180C/180C	F	NiMo	4.74	17.00	N/A	N/A
17	0.09	27C/27C	E	NiMo	1.31	2.27	2.12	4.04
18	0.09	27C/27C	F	NiMo	2.18	5.29	3.75	11.36
19	0.11	100C/100C	G	NiMo	1.96	3.69	3.54	7.59
20	0.11	100C/100C	H	NiMo	3.83	12.59	7.56	28.30
21	0.11	180C/180C	G	NiMo	2.91	6.30	6.08	15.57
22	0.11	180C/180C	H	NiMo	4.74	23.20	11.74	N/A
23	0.11	27C/27C	G	NiMo	1.48	2.54	2.43	4.59
24	0.11	27C/27C	H	NiMo	2.74	7.59	4.89	16.01
29	0.09	27C/27C	E	PT1	1.31	2.27	2.12	4.04
30	0.09	180C/180C	F	PT1	4.74	17.00	11.74	N/A
31	0.11	27C/27C	G	PT1	1.48	2.54	2.43	4.59
32	0.11	180C/180C	H	PT1	6.34	23.21	15.42	N/A
37	0.09	27C/27C	E	PT2	1.31	2.27	2.12	4.04
38	0.09	180C/180C	F	PT2	4.74	17.00	11.74	N/A
39	0.11	27C/27C	G	PT2	1.48	2.54	2.43	4.59
40	0.11	180C/180C	H	PT2	4.74	7.59	11.75	16.01

4.5 Prediction of Cooling Times for Dual Torch GMAW

Another application of the thermal analysis software was the torch distance analysis for dual torch welding procedure design.

During the plate welding design stage, the knowledge of appropriate range of torch distance for dual torch welding procedure was needed. It was for this reason that a set of thermal simulations of dual torch welding were performed. The purpose was to investigate the dependency of cooling times (T₈₅ and T₈₄) on torch distance for a fixed heat-input welding procedure.

4.5.1 The Dual Torch Welding Procedure

The baseline dual torch GMAW process under consideration was a 6-pass dual torch GMAW procedure. The basic welding parameters were listed in Table 18. To be decided in this procedure was the range of torch distance which can lead to the expected cooling times. With known weld metal responses to cooling times, the proper choice of torch distance would produce the right weld properties.

4.5.2 Simulation Results

Three torch distances were selected for the simulation: 50.8 mm (2 inches), 177.8 mm (7 inches), and 304.8 (12 inches). For all three cases, the pre-heat and inter-pass temperature was 180°C. The cooling times T_{85} in the HAZ of fill pass 1, a lead torch, were summarized for all three torch distances in

Table 19. Also included in the table are the “residual” temperatures by the lead torch right before the heating cycle by the trailing torch. The dependency of the cooling time T_{85} and the residual temperature on torch distance is quite significant, especially when the torch distance is less than 177.8 mm (7 in.). From 177.8 mm (7 in.) to 304.8 (12 in.), the impact of the torch distance becomes less visible.

Table 18. Welding parameters for dual-torch GMAW.

Pass No.	Voltage (V)	Current (A)	Wire Feed Speed (ipm)	Travel Speed (ipm)	CTWD (in)	Average Heat Input (kJ/in)	True Heat Input (kJ./in)
Hot Pass	26.3	244	480	18.3	1/2	21.1	24.1
FP1-L	27.7	231	480	18.3	1/2	21.0	23.9
FP2-T	25.4	235	480	18.3	9/16	19.5	22.8
FP3-L	27.2	229	480	18.3	1/2	20.4	23.8
FP4-T	25.4	227	480	18.3	9/16	18.9	22.5
Cap Pass	27.4	222	480	18.3	1/2	20.0	24.0

Table 19. Cooling time results for dual torch simulation.

Case No.	Torch Distance (in)	Dual Torch T_{85} (s)		Lead Wire Residual Temperature Before Trailing Torch (K)
		Lead	Trail	
1	2	N/A	21.7	1050 (777°C)
2	7	5.6	15.4	640(367°C)
3	12	5.3	12.3	585(312°C)

4.6 Simulation Results for Experimental Plate Welds

In preparing for weld metal Gleeble simulation, a number of experimental plate welds were made. For these welds, the bevel design was the same as the pipe bevel design for a girth weld. The welded plates were produced by flattening the pipes used in the first round welding.

The plate welds were made without any pre-heat and no true heat input data was recorded. The welding parameters are listed in Table 20. A unique feature of the welding procedure is that the heat input of the final fill pass of the weld is three times greater than those of the previous three fill passes. This was designed to produce pronounced variations within the weld so that Gleeble simulation samples with different microstructures could be produced. In the meantime, the large difference among weld passes within a girth weld certainly provides a good opportunity to test the robustness and versatility of the thermal model.

Table 20. Welding parameters for experimental plate weld.

Pass	Voltage (V)	Current (A)	Travel Speed (mm/min)	Heat Input (kJ/mm)
Hot Pass	25	188	1346.2	0.2
Fill Pass 1	24	185	508	0.5
Fill Pass 2	24	206	508	0.6
Fill Pass 3	23	194	508	0.5
Deep Fill	23	249	228.6	1.5

A thermal simulation was performed according to the welding conditions in Table 20. The macrograph of the weld and the peak temperature contour produced by the thermal model are shown in Figure 42. Without any parameter-tuning in the numerical model, the analysis tool was able to predict the thermal profile of the weld. The model robustness and consistency were proven again.

This simulation also provided useful information for microstructure characterization of the initial weld metal in the Gleeble simulations.

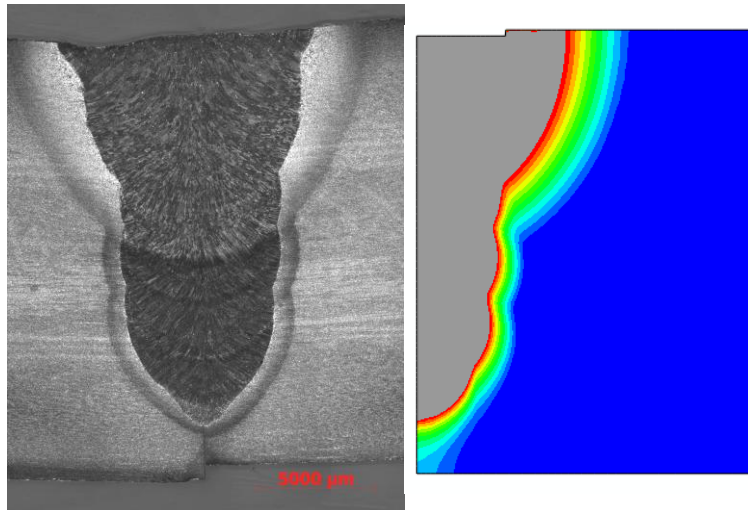


Figure 42. Macrograph (left) and predicted weld profile (right) by thermal model for experimental plate weld.

5 Concluding Remarks

For the welding of X100 linepipe steels, the identification of essential variables is critical to establish a viable range of welding conditions so that the required mechanical properties of the weld can be met. In addition to the conventional essential variables such as heat input, pre-heat and inter-pass temperatures, electrode consumable, and shielding gas, etc., the multi-wire GMAW variants added more welding variables and some of them may emerge as essential variables.

In the process of identifying these essential variables, a thermal analysis procedure has been developed and verified against a large amount of measured thermal cycle data. This procedure was also implemented through finite element method as a stand-alone analysis software tool.

5.1 Thermal Modeling of Multi-Pass, Multi-Wire P-GMAW Process

The thermal analysis procedure was developed and verified against a number of thermal cycle data sets, including the data by Hudson, the measurement data from the first round welds, and the measurement data from the second round welds. The procedure can simulate not only the traditional single-wire GMAW process but also the multi-wire GMAW variants.

Through a new heat flux formulation that combined the modified Goldak model with the moving-source solution in the characterization of the transient properties of the electrode, the thermal model demonstrated its accuracy, consistency, and robustness in its applications to the targeted welding processes with a wide range of heat inputs.

After its calibrations and verifications, the thermal analysis tool was used in the project research work to assist welding procedure design. In the process of identifying essential variables, it served as the primary analysis tool in performing the series of virtual experiments. It was also used to perform torch distance (spacing) analysis that gave further information related to welding procedure design.

5.2 Impact of True Heat Input

For P-GMAW processes, measurement data and weld property evaluation has shown that the true heat input instead of the averaged heat input ought to be considered if an accurate assessment of welding procedure is pursued. The experience of model development and calibration has confirmed the importance of true heat input, i.e., thermal simulation for P-GMAW using averaged heat input always under-predicted the peak temperature of the thermal cycle while using an “elevated” (true) heat input produced thermal cycles with satisfactory peak temperatures.

5.3 Characteristics of Thermal Cycles in Multi-wire P-GMAW

The thermal analysis procedure revealed that the thermal cycles in a multi-wire GMAW process are rather complicated. Depending on the locations within weld metal or HAZ, and the welding sequence, a multi-heating-cooling thermal cycle can have many combinations of peak temperatures, each of which can lead to different microstructure responses and therefore different weld properties. In a dual torch GMAW process analysis, for instance, the thermal model showed how torch distance (spacing) affects the cooling times.

5.4 The Thermal Analysis Tool

Because the thermal analysis procedure was implemented as a stand-alone software tool, it offers several advantages compared to using a commercial finite element package:

- 1) It automated a complicated modeling procedure, including the integration of the thermal model with a microstructure model. Some of the modeling steps, such as weld partitioning and meshing for a multi-pass girth weld, are very time-consuming if performed without an automation procedure;
- 2) As the direct results of procedure automation, the analysis tool is highly efficient and not error-prone at all compared to a manual process of model development;
- 3) Because it is written in generic finite element method, new features can be readily incorporated and implemented in the procedure.

6 References

- 1 Rosenthal, D. "Mathematical theory of heat distribution during cutting and welding," *Welding Journal*, p220s-234s, 1941.
- 2 Tsai, N., *Heat Distribution and Weld Bead Geometry in Arc Welding*, Ph. D., thesis, MIT, Massachusetts, 1983.
- 3 Wells, A., "Heat flow in welding," *Welding Journal*, 31(5), p263s-267s, 1952.
- 4 Malmuth, N. D., Hall, W. F., Davis, B. I., and Rosen, C. D., "Transient thermal phenomena and weld geometry in GTAW," *Welding Journal*, 53(9), p388s-400s, 1974.
- 5 Gosh, R. J., Trabant, E. A., and Hawkins, G. A., "Temperature distribution in solids of variable thermal properties heated by moving heat source," *Quarterly Appl. Mech.*, 13(2), p161-167, 1955.
- 6 Chen, Y., Zacharia, T., and David, S., "Heat transfer and fluid flow in gas metal arc weld pool with arc-pool interaction," *Proc. of the AWS convention*, Los Angeles, CA, April, 1997.
- 7 Zhang, W., Kim, C.-H., and DebRoy, T., "Heat transfer and fluid flow in welds with complex geometry during gas-metal arc fillet welding, Part I: Numerical model", *Journal of Applied Physics*, 95, p5210-5219, 2004.
- 8 Needham J.C., "Control of transfer in aluminium consumable electrode welding" Proceedings of the Physics of the Welding Arc Symposium, The Welding Institute, London, 114-122, 1962.
- 9 Yapp, D. and Blackman, S. A., "Recent Development in High Productivity Pipeline Welding," *J. of the Braz. Soc. of Mech. Sci. & Eng.*, 26(1), pp89-97, 2004.
- 10 Hudson, M., *Welding of X100 pipeline*, Ph. D. Thesis, Cranfield University, Cranfield, Beds (2004).
- 11 API 1104 (1999). Welding of pipelines and related facilities, 19th Edition, September 1999, publ. by American Petroleum Institute.
- 12 Rajan, V.B., "Essential Welding Variables", Final Report 278-T-06 to PHMSA per Agreement # DTPH56 07 T 000005, September 2011.
- 13 Sharma, A., Arora, N., and Gupta, S. R., "Simulation of effect of weld variables on thermal cycles during twin wire welding," *Proceeding of the 7th International Conference on Trends in Welding Research*, Pine Mountain, Georgia, USA, May 16-20, 2005.
- 14 Chen, Y., Wang, Y.-Y., Quintana, M.A., Rajan, V.B., and Gianetto, J.A. "Microstructure Model for Welding Simulations", Final Report 278-T-08 to PHMSA per Agreement # DTPH56 07 T 000005, September 2011.
- 15 Goldak, J., Chakravarti, A, and Bibby, M., "A new finite element model for welding heat sources," *Metallurgical Transactions B*, volume 15B, p587-600, 1984.
- 16 Chen, Y., Rudland, D. and Wilkowski, G., "Impact of Welding Sequence on the CRDM Nozzle-to-Vessel Weld Stress Analysis," Proceedings of ASME/JSME Pressure Vessels and Piping Conference, Hyatt Regency, La Jolla at Aventine, San Diego, California, July 25 – 29, 2004.
- 17 Touloukian, Y. S., Powell, R. W., Ho, C. Y., and Klemens, P. G., *Thermophysical Properties of Matters*, IFI/Plenum, 1970.
- 18 Reddy, J. N. and Gartling, D. K., *The Finite Element Method in Heat Transfer and Fluid Dynamics*, CRC Press, 1994.
- 19 Voller, V. R. and Swaminathan, C. R., "General source-based method for solidification phase change," *Numer. Heat Transfer* 19 175–8, 1991.
- 20 Panday, R. and Daniel, J., "Materials Selection, Welding And Weld Monitoring", Final Report 278-T-02 to PHMSA per Agreement # DTPH56 07 T 000005, September 2011.